Facilely prepared thirsty granules arouse tough wet adhesion on over-moist wounds for hemostasis and tissue repair

Li Xiong [a, 1], Huan Wang [b, 1], Junsu Wang [c], Jinyang Luo [a], Ruiqi Xie [a], Fei Lu [a], Guangqian Lan [a], Liang-Ju Ning [d, *], Rong Yin [e, *], Wenyi Wang [f, *], Enling Hu [a, g, *]

[a] State Key Laboratory of Resource Insects, College of Sericulture, Textile and Biomass Sciences, Southwest University, Chongqing 400715, China

[b] Winner Medical Co., Ltd., Shenzhen 518131, China

[c] Chongqing Customs Technology Center, Chongqing 400044, China

[d] Department of Orthopedic Surgery and Orthopedic Research Institute, Laboratory of Stem Cell and Tissue Engineering, State Key Laboratory of Biotherapy, West China Hospital, Sichuan University, Sichuan 610041, China

[e] Textile Engineering, Chemistry and Science, Wilson College of Textiles, North Carolina State University, Raleigh, NC 27695, USA

[f] Department of Applied Biology and Chemical Technology, The Hong Kong Polytechnic University, Hong Kong

[g] School of Fashion and Textiles, The Hong Kong Polytechnic University, Hong Kong

[1] These authors contributed equally to this work.

[*] Corresponding authors:

Liang-Ju Ning, ninglj@scu.edu.cn;

Rong Yin, ryin@ncsu.edu;

Wenyi Wang, wang.wenyi@polyu.edu.hk; and

Enling Hu, enling.allen.hu@connect.polyu.hk

Postal address:

Dr Enling Hu

School of Fashion and Textiles,

Room QT715, Q Core, 7/F,

The Hong Kong Polytechnic University,

Hung Hom, Kowloon, Hong Kong

ABSTRACT

Bioadhesives have been widely used in hemostasis and tissue repair, but the over- moist and wet nature of wound surface (due to the presence of blood and/or wound exudate) has led to poor wet adhesion of bioadhesives, which interrupts continuous care of wounds. Here, a thirsty polyphenolic silk granule (*Tan@SF-pwd-hydro*), which absorbs blood and exudate to self-convert to robust bioadhesives (*Tan@SF-gel-hydro*) *in situ*, was facilely developed in this study for enhanced wet-adhesion towards hemostasis and tissue repair. *Tan@SF-pwd-hydro* could shield wounds' wetness, and immediately convert itself to *Tan@SF-gel-hydro* to seal wounds for hemorrhage control and wound healing. The maximum adhesiveness of *Tan@SF-gel-hydro* over wet pigskin was as high as 59.8 ± 2.1 kPa. *Tan@SF-pwd-hydro* is a promising transformative dressing for hemostasis and tissue repair, since its hemostatic time was approximately half of that of the commercial hemostatic product, Celox ™, and its healing period was much shorter than that of the commercial bioadhesive product, Tegaderm ™. This pioneering study utilized the adverse wetness over wounds to arouse the robust adhesiveness by converting thirsty granules to bioadhesives *in situ*, creatively turning adversity into opportunities. The facile fabrication approach also offers new perspectives for manufacturing sustainability of biomaterials.

KEYWORDS

Bioadhesives, Wet adhesion, Hemostasis, Tissue repair, Silk

1 INTRODUCTION

Bleeding is one of the most common clinical indicators of injury. Blood loss of up to 30% of the total blood volume in the body could be deadly [1]. More than 85% of deaths are directly caused by uncontrolled bleeding that occurs in armed conflicts, accidents, or natural disasters [2]. In addition, 5.8 million individuals die annually from uncontrolled bleeding, with 30% of these deaths being trauma-related [3]. Notably, since hemostasis within 10 min of the onset of bleeding is crucial for reducing mortality, the development of quick hemostatic materials has recently garnered enormous interest [4].

Despite possessing hemostatic capacity, traditional hemostatic dressing materials such as zeolite, chitosan, alginate and gelatin sponge have disadvantages that should not be overlooked. Microporous zeolites, for instance, are not biodegradable and must be debrided correctly [5]. Similarly, chitosan hydrogels have hemostatic and antibacterial properties, but their poor tissue adherence and moderate hemolysis limit their widespread utilization [6]. Alginate is a good candidate for hemostasis, but its weak mechanical strength and chemical instability limit its use in severe hemorrhage control [7]. In addition, the poor adhesion of traditional dressing materials to the wound necessitates the employment of a fixing device, such as a bandage, for binding them to the bleeding tissue [8]. This potentially causes hemostatic dressings to slip and fall off the wound, decreasing the hemostatic effect. In addition to hemostasis, tissue repair following hemostasis is essential for both standard wound care and emergency

treatment [9]. Therefore, there is an immediate need for durable adhesive dressings for ongoing wound care in terms of both hemostasis and wound healing.

In response to the poor adhesion of conventional dressing materials, bioadhesives have gained significant interest in hemostasis recently. Hemostasis could also be fulfilled by physical sealing of bleeding wounds with adhesives rather than triggering coagulation cascade [10]. Unlike conventional dressings, bioadhesives close wounds quickly for hemostasis and wound healing, without the need for additional fixing devices. Much effort has been made in the developing of bioadhesives for wound care purposes. For instance a protein-based bio-glue with exceptional adhesion strength comparable to that of commercial cyanoacrylate superglue has been created by using electrostatically complexing cationic peptides with anionic aromatic surfactants [11]. A filamentous methacrylate bio-sealant with exceptional adherence [12] and a bio-inspired mucoadhesive hydrogel adhesive consisting of sodium alginate, gelatin, and protocatechuic aldehyde have also been developed [13]. Collectively, these researches support the notion that great progress has been made in bioadhesives to improve wound sealing.

However, bioadhesives have a number of disadvantages. First, blood flowing from wounds and wound exudates would adversely affect their sticking capabilities. This phenomenon occurs because biofluids inhibit direct contact between the bioadhesive

and the wound substrate [14]. Bioadhesives could also become detached from wounds due to hydro infiltration from wound exudate or blood, resulting in failure of hemostasis or wound healing. Thus, wet adhesion to tissues is extremely significant for bioadhesives. In addition, the synthesis of most existing bioadhesives involves the use of non-biosafe synthetic materials or harmful solvents. For example, cyanoacrylates-based tissue adhesives are broadly used [15]. But their degradation products could induce severe adverse effects [16].Likewise, Tissue Glu, a synthetic polyurethane tissue adhesive, was efficacious in reducing fluid accumulation [17]. However, it could also lead to potential complications [18]. These shortcomings make the majority of synthetic bioadhesives suitable for topical wounds only [5].

The use of bio-safe bioadhesives made of natural raw materials and green solvents is an effective way to avoid possible risks arising from synthetic materials. As a typical natural protein biopolymer, silk fibroin (SF) has been widely explored for medical applications [19]. However, the preparing of SF biomaterials is generally complicated and time-consuming [20]. Therefore, the invention of a facile preparation process for bio-safe silk bioadhesives could be of significance. Pristine SF itself has poor intrinsic adhesiveness but fortunately the abundant functional groups present in the composition of amino acids could allow the functionalizing of SF to serve as versatile biomaterials [21]. Thus, the functionalization of SF with specific small molecules towards wet adhesiveness is a feasible approach to endow SF composites with adhesiveness.

Small molecules and polymers that could provide adhesive groups to bioadhesives have been investigated for years. For example, gelatin methacryloyl (GelMA) and silk fibroin (SF) were used to prepare a biomaterial-based patch with adhesive and antimicrobial properties for wound healing in stretchable areas of the body [22]. A robust hemostatic bioadhesive (CAGA) with end-grafted abundant catechol was prepared. A levan-based adhesive hydrogel for hemostatic and wound healing was fabricated by conjugating catechol to levan [23]. The functionalization for adhesive capacities with these polyphenolic groups has been extensively proved elsewhere, which is the leading strategy to acquire bioadhesiveness [24]. Therefore, polyphenols shall also assist SF to anchor to tissues. Tannic acid (TA), a natural material extracted from plants, contains numerous polyphenolic groups. Thus, it could be expected that integration of TA with SF shall generate bio-safe bioadhesives.

Tan@SF-pwd-hydro, a granular thirsty wound dressing with fast self-gelling by hydro-stimulation and strong wet adhesion for wound care, was developed in this study. The *Tan@SF-pwd-hydro* substance was created in the following steps (Figure 1A): 1) silk fibroin (SF) was mixed with TA to produce adhesive *Tan@SF-gel*, which was the precursor of *Tan@SF-pwd-hydro*; 2) *Tan@SF-pwd* was produced by freeze-drying and grinding *Tan@SF-gel*; 3) *Tan@SF-pwd-hydro*, which displayed improved hydrophilicity and water conductivity compared with *Tan@SF-pwd*, was produced by

simply doping *Tan@SF-pwd* with PEG [25]. When applied to bleeding wounds, *Tan@SF-pwd-hydro* rapidly absorbed blood or exudate to create adhesive *Tan@SF-gel-hydro* in situ, which not only formed a stable physical barrier to stop bleeding, but also protected the wounded site to encourage tissue repair (Figure 1B).

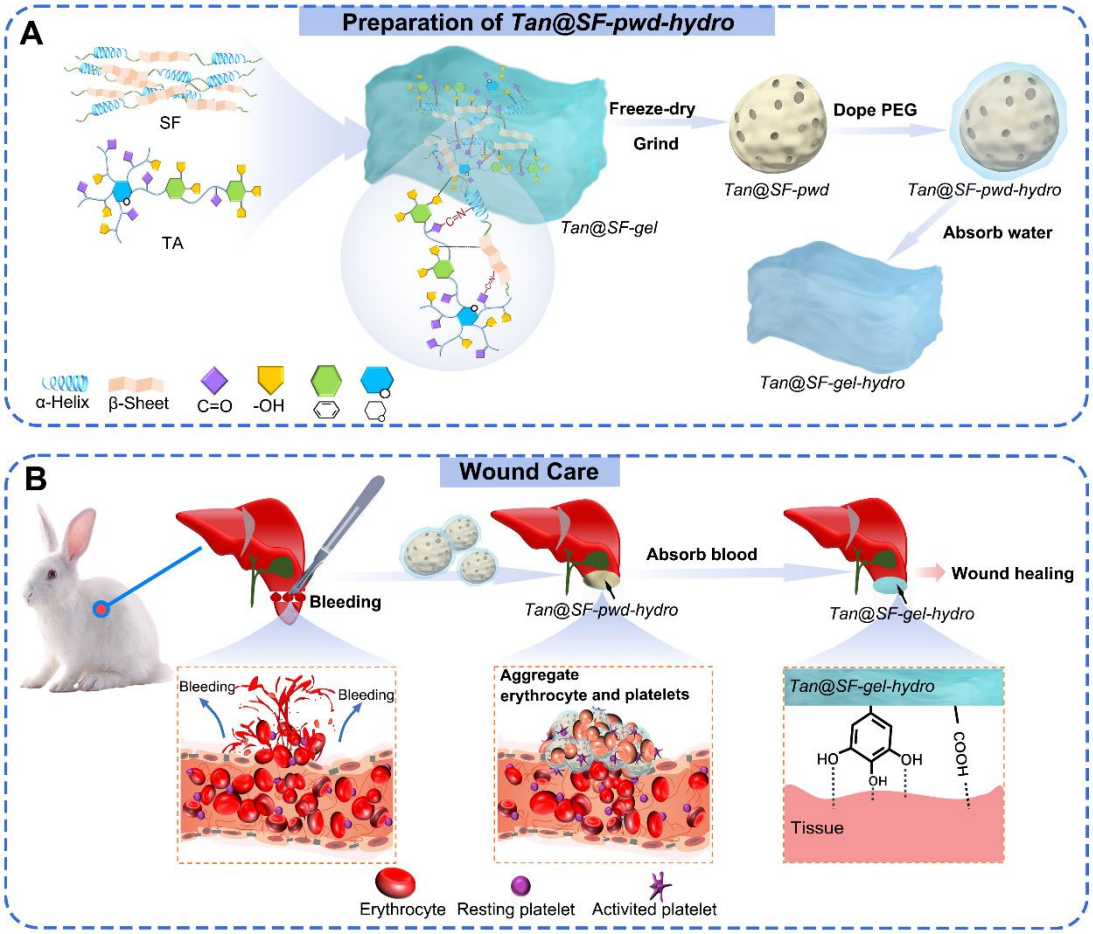

Figure 1. A) Preparation of *Tan@SF-pwd-hydro*. B) Wound care with *Tan@SF-pwd-hydro.*

Tan@SF-pwd-hydro offers significant benefits over conventional dressing materials. First, the hydrophilic thirsty *Tan@SF-hydr-pwd* could eliminate interfacial water on

wounds to provide a suitable dry milieu for robust wet adhesion, thereby transforming the negative effects of the wetness of wounds into a positive stimulant for the forming of bioadhesive. Second, granular *Tan@SF-pwd-hydro* was more fillable and naturally adaptable to the intricate wound profile to seal wounds flawlessly for hemostasis and healing. Third, it would be easier to transport and store *Tan@SF-gel-hydro* in its dry state than adhesive hydrogels with ultra-high water content [26]. Fourth, and most importantly, the preparation method in this study utilized an ultra-clean and quick approach.

2 EXPERIMENTAL

2.1 Materials and Reagents

Bombyx mori cocoons were provided by High Fashion International Limited (New Territories, Hong Kong). TA was purchased from Shanghai Macklin Biochemical Co., Ltd. PEG was obtained from Chengdu Kelong Chemicals Co., Ltd. Female New Zealand white rabbits were used for evaluation of *in vivo* biocompatibility and hemostasis and wound healing. All animal experiments were approved by the National Center of Animal Science Experimental Teaching at the College of Animal Science and Technology, Southwest University, China (Approval No.: LAC2023-1-0228), and met the requirements of the Guide for the Care and Use of Laboratory Animals.

2.2 Preparation of *Tan@SF-pwd-hydro*

First, degummed silk fiber was dissolved in a ternary solution ($CaCl_2/C_2H_5OH/H_2O$ with a molar ratio of 1:2:8) at 80 °C for 2 h with a bath ratio of 1:10. Following dialysis, the silk solution was combined with a TA solution, with the concentrations of SF and TA in the resulting combination set at 3% and 2% (Figure S1), respectively, in order to produce precipitates (*Tan@SF-gel*) immediately (Movie S1). After freeze-drying and grinding, *Tan@SF-gel* was converted to *Tan@SF-pwd*, which could return to *Tan@SF-gel* again by absorbing water. To increase the hydrophilicity and hydraulic conductivity of *Tan@SF-pwd*, PEG was evenly doped with *Tan@SF-pwd* to prepare the thirsty granules (*Tan@SF-pwd-hydro*) that could absorb water to form the final bioadhesive (*Tan@SF-gel-hydro*) for wound care.

2.3 Characterization

Scanning electron microscopy (SEM), Fourier-transform infrared spectroscopy (FTIR), X-ray diffraction (XRD), proton nuclear magnetic resonance (^{1}H NMR) and X-ray photoelectron spectroscopy (XPS) were used for material characterization.

2.4 Evaluation of Water Retention and Blood Absorption and Self-healing Performance

Water retention, and water and blood absorption ratio were measured according to a previously published report with minor revision [27]. The applied temperature was set at 37 ℃. In the self-healing evaluation, two sections of *Tan@SF-gel-hydro* (thickness: 3

mm; diameter: 10 mm), which were cut from a single intact substrate and which were stained differently, were stacked to examine their self-healing capacity.

2.5 Adhesion Tests

(1) Determination of adhesion potentials

The adhesion strength and adhesion repeatability of *Tan@SF-pwd-hydro* were examined by the lap shear test. *Tan@SF-pwd-hydro* (0.1 g) was spread uniformly on a wet pigskin to produce *Tan@SF-gel-hydro* (spreading size: 15 mm × 15 mm). The wet pigskin was bonded to another piece of pigskin with identical specifications and then allowed to rest for 20 min before being stretched on a universal stretching machine (stretching speed: 5 mm/min). There were 5 rounds of measurement in total. In the adhesion repeatability evaluation, 50 stretches were performed in each round.

The interfacial toughness and adhesion energy were measured by T-shape peeling test. *Tan@SF-pwd-hydro* (0.1 g) was spread uniformly on a wet pigskin to produce *Tan@SF-gel-hydro* (spreading size: 15 mm × 30 mm). The pigskin was bonded to another piece of pigskin with identical specifications and then allowed to rest for 20 min before using the universal stretching machine (stretching speed: 24 mm/min). The measurement was conducted 5 times in total.

The bursting pressure was measured using a self-assembled bursting apparatus. In the center of a 30 mm-diameter pigskin disc, a 3 mm-diameter round hole was formed. Prior to being coupled to the bursting device, the pigskin disc was sealed with *Tan@SF-gel-hydro*, which was converted from *Tan@SF-pwd-hydro* (0.1 g) by water absorption. The phosphate buffer saline (PBS) was then fed into a booster to gradually increase the interior pressure of the device. The bursting strength of *Tan@SF-gel-hydro* was recorded as the highest pressure. Each specimen was examined 5 times.

(2) Adhesion stability and underwater adhesiveness

To determine the adhesive stability to various organs (pig skin, heart, liver, kidney and small intestine) in water, *Tan@SF-pwd-hydro* was applied uniformly to wet tissues to generate adhesive *Tan@SF-gel-hydro*. After submerging the *Tan@SF-gel-hydro*-adhered tissues in water, they were spread, bent, twisted, and then irrigated with flushing water to assess the adhesive stability.

To examine the ability to seal injured tissues, PBS was injected into a closed segment of pig intestine, which was subsequently pierced to allow the smooth flowing out of the fluid. *Tan@SF-pwd-hydro* was then uniformed applied to the wet intestine for sealing, after which the intestine was refilled with PBS to assess the leaking/sealing status.

To evaluate the underwater adhesion, a piece of pigskin was submerged in water with one end weighted (50 g) and the other end covered with *Tan@SF-gel-hydro*. A second piece of pigskin was subsequently attached to the *Tan@SF-gel-hydro*-coated end of the initial pigskin under water. Soon, the opposite end of the second pigskin would be hoisted to pull the first pigskin out of the water to test the adhesion of *Tan@SF-gel-hydro*.

(3) Adhesion under harsh conditions

The lap shear test was used again to determine the adhesion strength with various fluids. *Tan@SF-pwd-hydro* (0.1 g) was uniformly distributed over a piece of dry pigskin (spread size: 15 mm×15 mm). The granular *Tan@SF-pwd-hydro* was then transformed into *Tan@SF-gel-hydro* by adding drops of different fluids.The dry pigskin was then attached to another piece of pigskin of the same size. Blood, simulated intestinal fluid (SIF), simulated body fluid (SBF), simulated sweat fluid (SSF), simulated gastric fluid (SGF), and simulated seawater fluid (SWF); NaCl, KCl, $CuCl_2$, $MgCl_2$, and $CaCl_2$ solutions (2.5 M); and aqueous solutions of pH 1, pH 3, pH 5, pH 7, pH 9, pH 11 and pH 13 were utilized.

In the adhesion assessment at harsh temperature, *Tan@SF-pwd-hydro* was first stored at various temperatures for 48 h before being spread onto a piece of wet pigskin to produce *Tan@SF-pwd-hydro* for bonding to another piece of pigskin. The adhesion

strength was immediately assessed following the attachment of the two pieces of pigskin.

2.6 Biocompatibility Assessment

The biodegradation performance of samples (50 mg) was evaluated using a subcutaneous implantation model of New Zealand rabbits [19]. At the desired intervals (2, 4, 8, 12, 16 weeks), the rabbits were sacrificed to collect the tissue surrounding the implantation site for histological analysis. L929 Mouse fibroblast cells were used to test the cytotoxicity [28]. The hemolysis rate was tested according to a previous work [29]. Samples (15 mg) dispersed in erythrocyte suspension (5%, 3 mL) were incubated in a shaker at 37 ℃ for 1 h before testing.

2.7 Determination of Blood Coagulation Index

The blood coagulation index (BCI) was determined according to a previous study [16]. The concentration of $CaCl_2$ used was 0.22 M.

2.8 Assessment of Erythrocyte and Platelet Adhesion

Erythrocyte and platelet adhesions were observed based on previously published reports with slight modifications [30].

To measure the erythrocyte adhesion number, anticoagulated whole blood (5 mL) was added to PBS (10 mL) and centrifuged for 10 min at 1,500 rpm to extract erythrocytes. *Tan@SF-pwd* or *Tan@SF-pwd-hydro* (25 mg) was then mixed with erythrocyte suspension (5%, 200 μL) and incubated at 37 ºC for 30 min. The attached erythrocytes on samples were then rinsed 3 times with PBS and transferred to deionized water (3 mL) to lyse the attached erythrocyte for 1 h at 37 ℃. The absorbance of the lysate solution (A_{sample}) was measured at the wavelength of 545 nm using a UV-Vis spectrophotometer. The erythrocyte adhesion number was calculated using Equation (1):

$$\text{Erythrocyte adhesion number} = \frac{N_{blood} \times A_{sample}}{A_{blood}} \qquad \text{Equation (1)}$$

Wherein, N_{blood} is the full number of erythrocytes in anticoagulated whole blood (1 mL), and A_{blood} is the absorbance of anticoagulated whole blood at the wavelength of 545 nm.

To measure the platelet adhesion number, a lactate dehydrogenase (LDH) assay was performed. The platelet-rich plasma (PRP) was obtained by centrifuging anticoagulated whole blood at 1,500 rpm for 10 min. *Tan@SF-pwd* or *Tan@SF-pwd-hydro* (25 mg) was then added to PRP (200 uL) and the mixture was incubated for 30 min at 37 ℃. Next, samples that rinsed with PBS was added with Triton X-100's PBS (1%, 0.3 mL) to lyse the attached platelets for 1 h at 37 ℃. Thereafter, the released LDH from the

lysis of platelets was detected using an LDH kit. A calibration curve was obtained by measuring the optical density at the wavelength of 440 nm to determine the number of attached platelets.

2.9 Evaluation of *in vivo* Hemostasis

Female New Zealand rabbits were utilized in the ear artery and liver bleeding models to demonstrate the hemostatic capability of samples. A 10 mm incision was made in the ear artery and in the liver of the rabbits to induce bleeding. Immediately, samples (0.25 g) were put directly on the bleeding locations and promptly pressed with medical gauze. The gauze was then carefully lifted to observe the bleeding status every 5 s. Following the cessation of bleeding, hemostatic time and blood loss were recorded. Celox ™, a commercially available hemostatic product, was used as the control. Before using Celox ™ for hemostasis, gushing blood over the wound was removed by medical gauze.

2.10 Evaluation of *in vivo* Wound Healing Assessment

The *in vivo* wound healing evaluation was conducted according to a reported work [31]. Excision of circular full-thickness skin (1.5 cm in diameter) was conducted on the back of New Zealand rabbits. When applying the thirsty *Tan@SF-pwd-hydro* or *Tan@SF-pwd* granules on wounds, no extra removal of superficial blood over bleeding wounds was performed. At the desired intervals, the rabbits were sacrificed to collect the tissue surrounding the implantation site for histological analysis. Tegaderm ™, a

commercially available adhesive dressing product, was used as the control. Before using Tegaderm ™ for wound healing, fresh blood and exudate over the wound were removed by medical gauze.

2.11 Statistical Analysis

Statistical analyses were performed using one-way analysis of variance. Differences were considered as statistically significant when the *P*-value was less than 0.05.

3 RESULTS AND DISCUSSION

3.1 Characterization

The surface morphologies of *Tan@SF-pwd*, *Tan@SF-gel*, *Tan@SF-pwd-hydro*, and *Tan@SF-gel-hydro* were shown in Figure 2A. Both *Tan@SF-pwd* and *Tan@SF-pwd-hydro* had micropores that were capable of absorbing water to form gels. These pores on the surface could be a result of the freeze-drying. *Tan@SF-gel-hydro* had a smoother surface than *Tan@SF-gel*, which could be due to the fact that the improved hydrophilicity of *Tan@SF-pwd-hydro* allowed for increased water absorption to improve its flowability. This merit of improved flowability could enable *Tan@SF-pwd-hydro* to completely fill wound gaps for effective hemostasis and tissue repair.

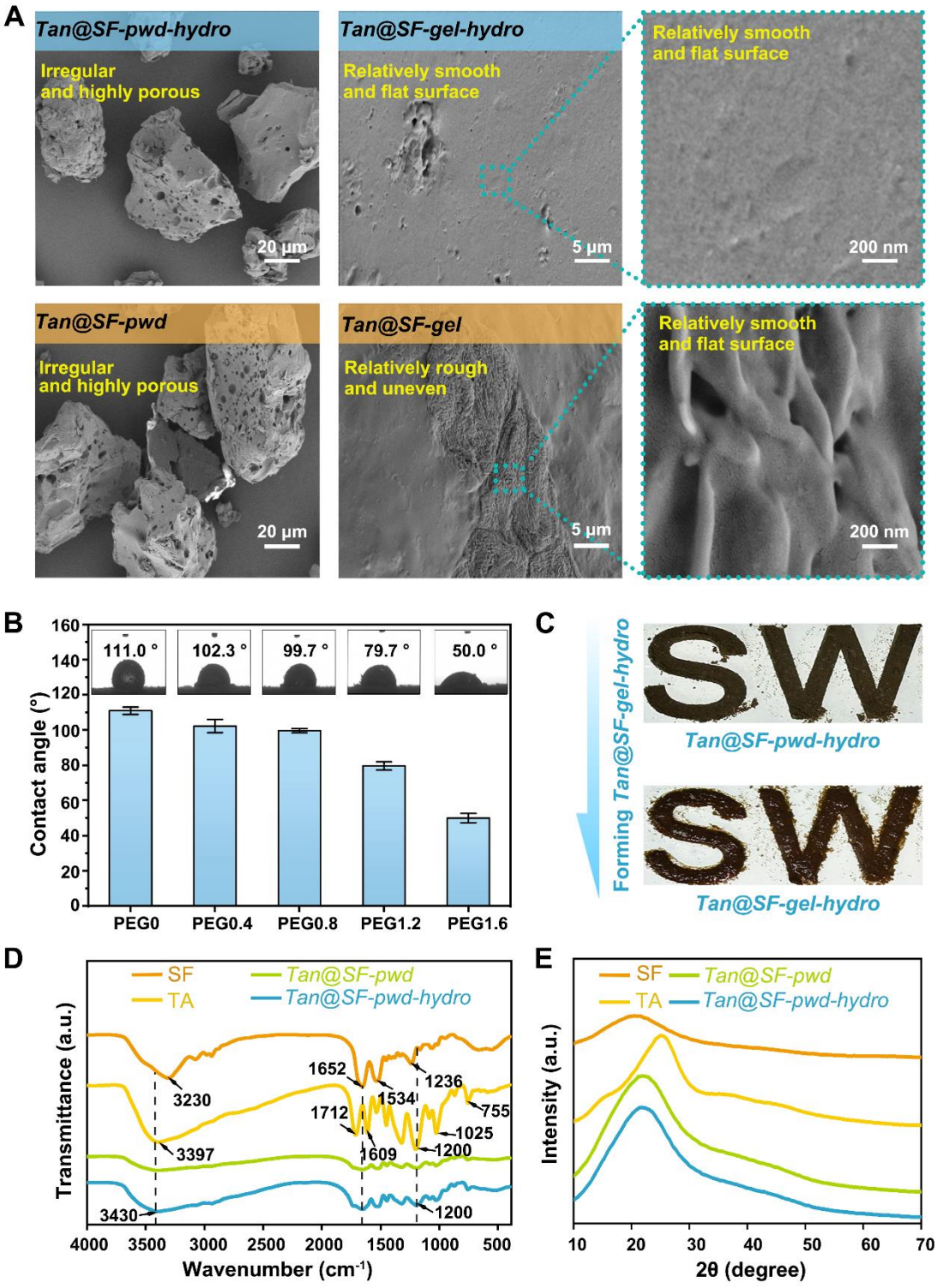

Figure 2. A) SEM images. B) Contact angles of *Tan@SF-pwd-hydro* doped with PEG in various dosages. C) Transformation of *Tan@SF-pwd-hydro* to *Tan@SF-gel-hydro.* D) FTIR spectra. E) XRD spectra.

The increased hydrophilicity of *Tan@SF-pwd-hydro* could be the result of doping *Tan@SF-pwd* with PEG, which had good water conductivity [32]. The influence of PEG dosage on the hydrophilicity of *Tan@SF-pwd-hydro* was analyzed by using the contact angles depicted in Figure 2B. *Tan@SF-pwd-hydro* without PEG (*Tan@SF-pwd*) had contact angles as high as 111.0 ± 2.1°. The contact angles of *Tan@SF-pwd-hydro* that had been doped with increasing dosage of PEG decreased significantly, reaching 50.0 ± 2.7° for the sample doped with 1.6% PEG. This was due to the fact that a suitable concentration of PEG doping might induce water into the interior of *Tan@SF-pwd-hydro* particles, hence speeding up water absorption. As an excess of PEG was observed to hinder the formation of *Tan@SF-gel-hydro*, the doping mass of PEG was fixed at 1.6% for the production of subsequent *Tan@SF-pwd-hydro* samples. Thanks to the enhanced hydrophilicity, the thirsty *Tan@SF-pwd-hydro* quickly converted into *Tan@SF-gel-hydro* when given water (Figure 2C).

Tan@SF-pwd-hydro was analyzed by FTIR spectra to identify the interactions between its components (Figure 2D). The TA spectrum showed a large peak of the -OH stretching vibration at 3397 cm^{-1}. The stretching vibrations of the C=O group of the aromatic ester, the aromatic C=C group, and the aromatic C-C group exhibited absorption bands at 1712 cm^{-1}, 1609 cm^{-1}, and 1530 cm^{-1}, respectively [33]. With the exception of a few peaks that were slightly displaced, *Tan@SF-pwd* and *Tan@SF-pwd-hydro* did not exhibit any new peaks in comparison to TA. *Tan@SF-pwd* merged the

broad peak at 3397 cm^{-1} in TA and the broad peak at 3230 cm^{-1} in SF to produce a rather flat broad peak at 3430 cm^{-1}. Due to the lack of new peaks, only non-covalent interactions were confirmed between TA and SF. The large peak at 3397 cm^{-1} of TA, the relatively small peak at 3230 cm^{-1} of SF, and the broad peak at 3430 cm^{-1} of *Tan@SF-pwd* indicated that *Tan@SF-pwd* formed a substantial number of intermolecular hydrogen bonds. In addition, a slight decrease from 1534 cm^{-1} (representing random curl) to 1521 cm^{-1} (representing β-sheet) was noticed [34], showing that the interaction between SF and TA triggered the conformational transition of SF from the random coil to β-sheet [35]. Since β-sheet in SF exhibited high inherent toughness and excellent wet adhesion performance [36], it was anticipated that *Tan@SF-pwd-hydro* containing a large amount of β-sheet would exhibit remarkable wet adhesiveness potential. The absence of new peaks in *Tan@SF-pwd-hydro* revealed that PEG doping in *Tan@SF-pwd* did not form any covalent bonds with *Tan@SF-pwd* and just altered the water conductivity.

Figure 2E shows the XRD pattern of all materials. The amorphous structure of TA was denoted by the diffraction peak at 25.19° [33]. At 20.9°, the peak of SF, which indicated the β-sheet in SF, was identified. In addition, the broad peak revealed the characteristic amorphous shape of SF. With the addition of TA, the *Tan@SF-pwd* peak shifted to the left, indicating an increase in the β-sheet structure that contributed to enhanced mechanical strength and adhesion of *Tan@SF-pwd* and *Tan@SF-pwd-hydro*. In

comparison to *Tan@SF-pwd*, the equivalent diffraction peak of *Tan@SF-pwd-hydro* did not shift, and no new derivative peaks were produced, indicating that doping *Tan@SF-pwd* with PEG did not modify its crystalline state. In addition, ^{1}H NMR analysis was performed on *Tan@SF-pwd* to confirm the presence of polyphenolic hydroxyl groups (trihydroxybenzene groups) that should be responsible for its adhesiveness. As shown in Figure 3A, polyphenolic groups were found in both TA and *Tan@SF-pwd* (δ= 7.3-6.9 ppm), indicating that polyphenolic groups were preserved to provide tissue-bonding capacity [35]. Thus, it was anticipated that *Tan@SF-gel-hydro* promised to fulfill wet adhesion to tissues at amino groups.

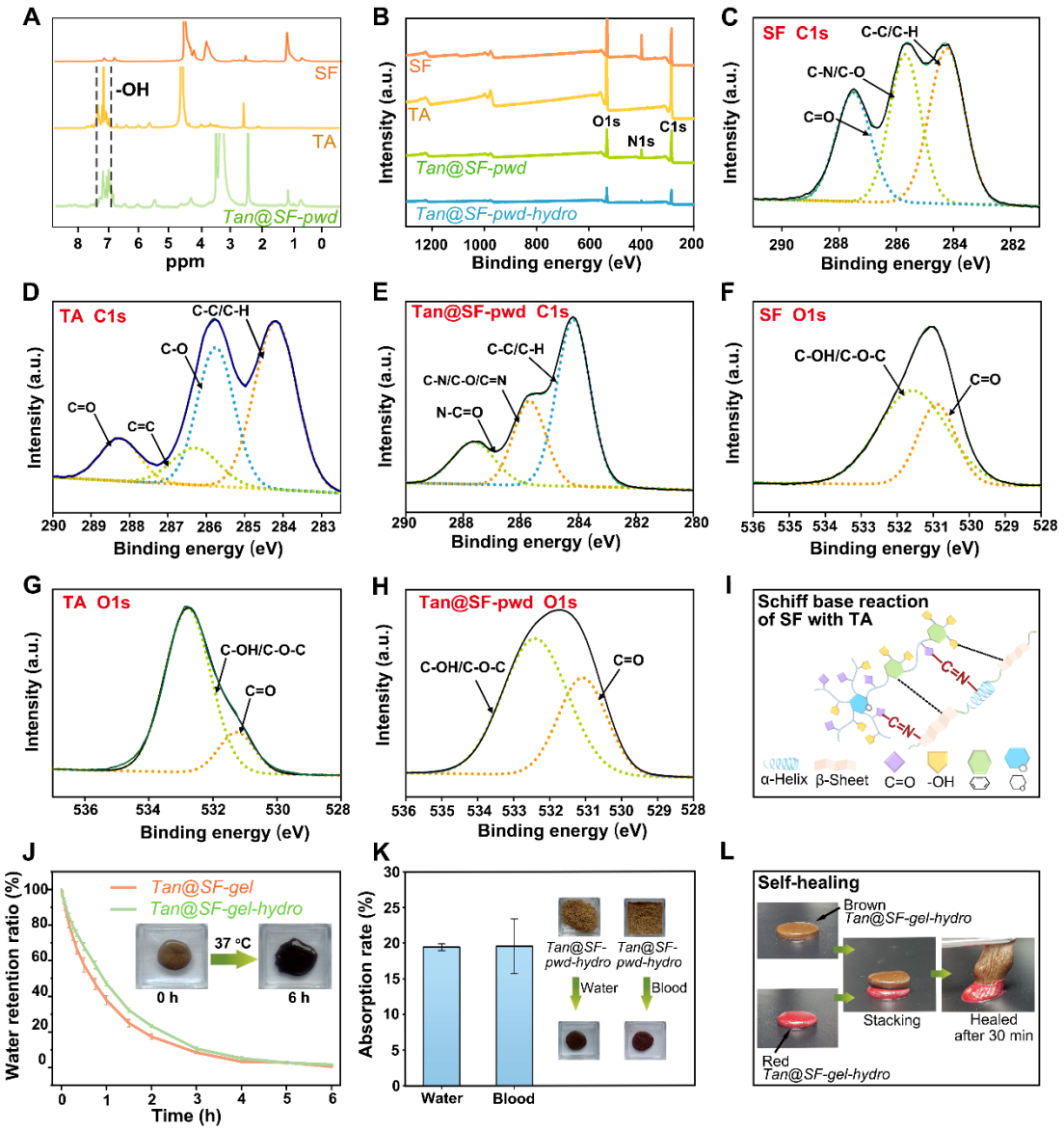

Figure 3. A) ^{1}H NMR spectra. B) Fullscale XPS spectra. C-H) High-resolution XPS spectra of C1s and O1s in SF, TA and *Tan@SF-pwd*. I) Schematic of Schiff base reaction between SF and TA. J) Water retention. K) Water- and blood-absorption of *Tan@SF-pwd-hydro*. L) Self-healing of *Tan@SF-gel-hydro*.

Figure 3B displays the XPS spectra of SF, TA, *Tan@SF-pwd*, and *Tan@SF-pwd-hydro*. Carbon and oxygen, two primary elements, were identified. Compared to SF, the proportion of carbon (285.1 eV) in *Tan@SF-pwd* reduced to 285.1 eV, but the

proportions of nitrogen (399.15 eV) and oxygen (532.38 eV) increased significantly, showing the binding of SF protein to TA. According to high-resolution XPS spectra of the chemical states of the main part (C1s) components in SF, TA, and *Tan@SF-pwd*, the three peaks at 284.2, 285.7, and 287.5 eV in the C1s spectra of SF corresponded to C-C/C-H, C-N/C-O, and C=O bonds, respectively (Figure 3C). Four peaks at 284.2, 285.7, 286.3, and 288.3 eV corresponded to C-C/C-H, C-O, C=C, and C=O bonds, respectively, in the spectra of TA (Figure 3D). The three peaks in *Tan@SF-pwd* at 284.2, 285.7, and 287.6 eV corresponded to C-C/C-H, C-N/C-O/C=N, and C=O bonds, respectively (Figure 3E). Wherein, the C=N bond in *Tan@SF-pwd* was predominantly produced by the Schiff base reaction between the amino group in SF and the aldehyde group in TA (Figure 3I) [37].

On the basis of high-resolution XPS spectra of the chemical states of the major component (O1s), peaks at 530.9 and 531.6 eV were ascribed to oxygen in the carbonyl group (C=O) and C-OH/C-O-C, respectively in SF (Figure 3F) [38]. While the peaks at 531.3 and 532.8 eV were mostly attributed to oxygen in the carbonyl group (C=O) and C-OH/C-O-C in TA (Figure 3G). In *Tan@SF-pwd*, due to the interaction between SF and TA, the C=O and C-OH/C-O-C peaks in SF and TA merged into a single peak (Figure 3H), which could be attributed to the oxidation of polyphenolic or carboxyl group and quinone or carbonyl group [39], further indicating cross-linking between TA and SF.

3.2 Water Retention, Water and Blood Absorption, and Self-healing

Adhesives could be susceptible to hydrated effects and frequently lose their adhesiveness as a result of water loss, preventing them from attaching to bleeding tissue [40]. Figure 3J depicts the water retention of *Tan@SF-gel-hydro* and *Tan@SF-gel* at 37 °C. Even though both *Tan@SF-gel-hydro* and *Tan@SF-gel* lost their water content after 5 h, this duration was already sufficient for hemostasis. *Tan@SF-gel-hydro* held water somewhat better than *Tan@SF-gel*, which could be explained by the presence of PEG in *Tan@SF-gel-hydro*, which hindered water evaporation from the *Tan@SF-gel-hydro* substrate.

Water and blood absorption were crucial properties because *Tan@SF-pwd-hydro* needed to absorb liquid to transform itself into an adhesive, while simultaneously shielding free water over moist tissue to generate strong adhesion. Figure 3K demonstrates *Tan@SF-pwd-hydro*'s water and blood absorption capacity. The water absorption rate of *Tan@SF-pwd-hydro* required to create *Tan@SF-gel-hydro* was 19.4 ± 0.5%, what was comparable to that of blood (19.6 ± 3.8%). This revealed the steady absorption capacity of *Tan@SF-pwd-hydro*.

During use, bioadhesives may be subjected to external mechanical forces, which may cause them to break and decrease their performance [41]. Therefore, bioadhesives must

possess substantial self-healing characteristics in order to provide durable protection for wounds. Figure 3L demonstrates that *Tan@SF-gel-hydro* was capable of self-healing. Two distinct *Tan@SF-gel-hydro* slices, which were cut from a single undamaged substrate and dyed with distinct colors, were stacked in the air. After a short while, the two *Tan@SF-gel-hydro* slices rejoined to form a single entity. This occurred because a large number of hydrogen bond donors and acceptors were exposed in the cross section when *Tan@SF-gel-hydro* was disrupted, allowing *Tan@SF-gel-hydro* to rapidly repair itself via hydrogen bonding upon re-contact [42]. This allowed *Tan@SF-gel-hydro* to self-repair damaged substrates and reserved functions during application, extending their service lives and avoiding additional maintenance expenses [43].

3.3 Adhesive Strength

Figure 4A depicts the lap-shear apparatus, while Figure 4B depicts the bearing pressure of *Tan@SF-gel-hydro* on pigskin. As the displacement grew, the lap-shear strength increased and then decreased until complete stretching was attained. The highest lap-shear strength was measured 34.2 kPa, which suggested that *Tan@SF-gel-hydro* and pigskin adhered well. Figure 4C depicts the adhesion strength of *Tan@SF-gel-hydro* when subjected to repeated cyclic stretching. The adhesive strength of *Tan@SF-gel-hydro* rose and then stabilized as the number of stretching cycles increased from 0 to 50. The adhesive strength attained a maximum of 59.8 ± 2.1 kPa after 40 cycles of stretching. Subsequently, there was not much change in the adhesion strength. This

showed that the repeated stretching might have caused a rearrangement of polymeric chains in *Tan@SF-gel-hydro*, hence improving its physical strength and adhesiveness. Moreover, the hydrogen bonding between cross-linked SF and TA might constitute a reversible physical contact that was more uniformly dispersed during continuous stretching, giving *Tan@SF-gel-hydro* a persistent and reproducible adhesion behavior [44].

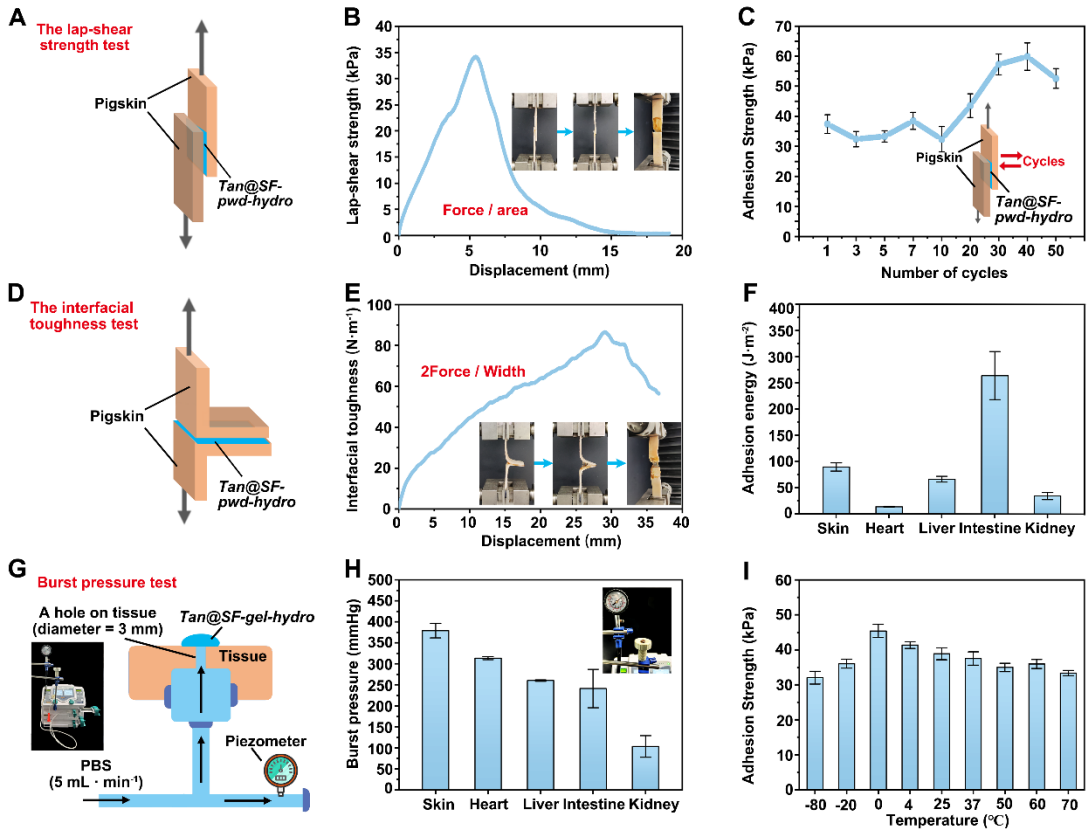

Figure 4. A) Schematic of lap-shear test. B) Lap-shear strength of *Tan@SF-gel-hydro*. C) Cyclic lap-shear strength of *Tan@SF-gel-hydro*. D) Schematic of peel test. E) Interfacial toughness of *Tan@SF-gel-hydro*. F) The adhesion energy of *Tan@SF-gel-*

hydro. G) Schematic of burst pressure test; H) Burst pressure of *Tan@SF-gel-hydro*; I) The adhesion strength of *Tan@SF-gel-hydro* at different temperatures.

The peel test, which measures the energy required to peel per unit width on the contact surface, is a common method for determining a material's adhesiveness [45]. Figure 4D depicts the peel test, and Figure 4E depicts the interfacial toughness of *Tan@SF-gel-hydro*. As the strength of displacement increased, the interfacial toughness initially increased and then decreased. The highest interfacial tensile strength achieved was 86.5 N/m. In addition, the adhesion energies of *Tan@SF-gel-hydro* were high when it was attached to pigskin, intestine, heart, kidney, or liver (Figure 4F). *Tan@SF-gel-hydro* was discovered to have the highest peel adherence on the intestine (282.5 ± 63.5 J/cm^2).

The burst pressure represents intermolecular cross-linking strength as well as tissue adhesion [46]. Stronger adhesiveness and toughness are associated with higher burst pressure. Figure 4G shows the bursting apparatus, while Figure 4H shows the bearing pressure. Pig skin, heart, liver, and small intestine all experienced burst pressure. The burst pressures on the pig skin, heart, liver and small intestine were 379.1 ± 17.2 mmHg, 313.7 ± 3.4 mmHg, 260.2 ± 1.7 mmHg and 241.3 ± 45.6 mmHg, respectively, which were significantly higher than the arterial blood pressure of humans (120.0 mmHg) [47]. *Tan@SF-gel-hydro* possessed exceptional wet adhesion capacity and tight

intermolecular cross-linking to seal bleeding wounds on diverse biological tissues without rupturing, as evidenced by its high burst pressure on diverse tissues.

3.4 Adhesion under harsh conditions

The evaluation of adhesive qualities in extreme conditions was essential. The impact of severe conditions on adhesive potential (before adhesion occurred) and adhesive stability (after adhesion occurred) was substantial. For example, a skater may get injured in a cold environment, necessitating the use of adhesive hemostatic materials that could maintain its adhesiveness at low temperatures [48]; similarly, an injured surfer may come into contact with seawater, necessitating the use of adhesive hemostatic materials that were resistant to seawater and kept their adhesive stability intact [49]. As a result, there was an urgent need to ensure that the adhesive could maintain its adhesion and durability in various severe settings, such as low temperature, high salt, and variable pH conditions.

For this, the adhesive strength of *Tan@SF-gel-hydro* to skin at different temperatures (-80, -20, 0, 4, 25, 37, 50, 60 ℃) was tested using the lap-shear test. As shown in Figure 4I, the maximum adhesive strength was achieved at 45.4 ± 4.9 kPa at 0 ℃, suggesting *Tan@SF-gel-hydro* could be used in the cold environment for injured skaters. The adhesive strength of *Tan@SF-gel-hydro* at other temperatures was slightly lower, but all over 32.0 kPa. This proved that temperature had no major effect on the adhesiveness

of *Tan@SF-gel-hydro*. Thus *Tan@SF-gel-hydro* could be applied regardless of temperature variations because its adhesiveness was observed to be satisfactory throughout a broad temperature range.

Figure 5A displays the adhesive strength of *Tan@SF-gel-hydro* in simulated fluids. *Tan@SF-gel-hydro* exhibited significant adhesiveness in SGF of up to 63.4 ± 1.2 kPa. This indicated that *Tan@SF-gel-hydro* could be used to seal perforated stomach for hemorrhage control or tissue amendment. Moreover, the adhesive strength in SWF was as high as 56.5 ± 2.6 kPa. It was probable that the Ca^{2+} and Mg^{2+} in seawater acted as ligand ions to increase the cohesion of *Tan@SF-gel-hydro* [50]. This suggested that *Tan@SF-gel-hydro* could be effective for emergency hemostasis among fishermen and sailors who were likely to be exposed to seawater in their daily lives or at work.

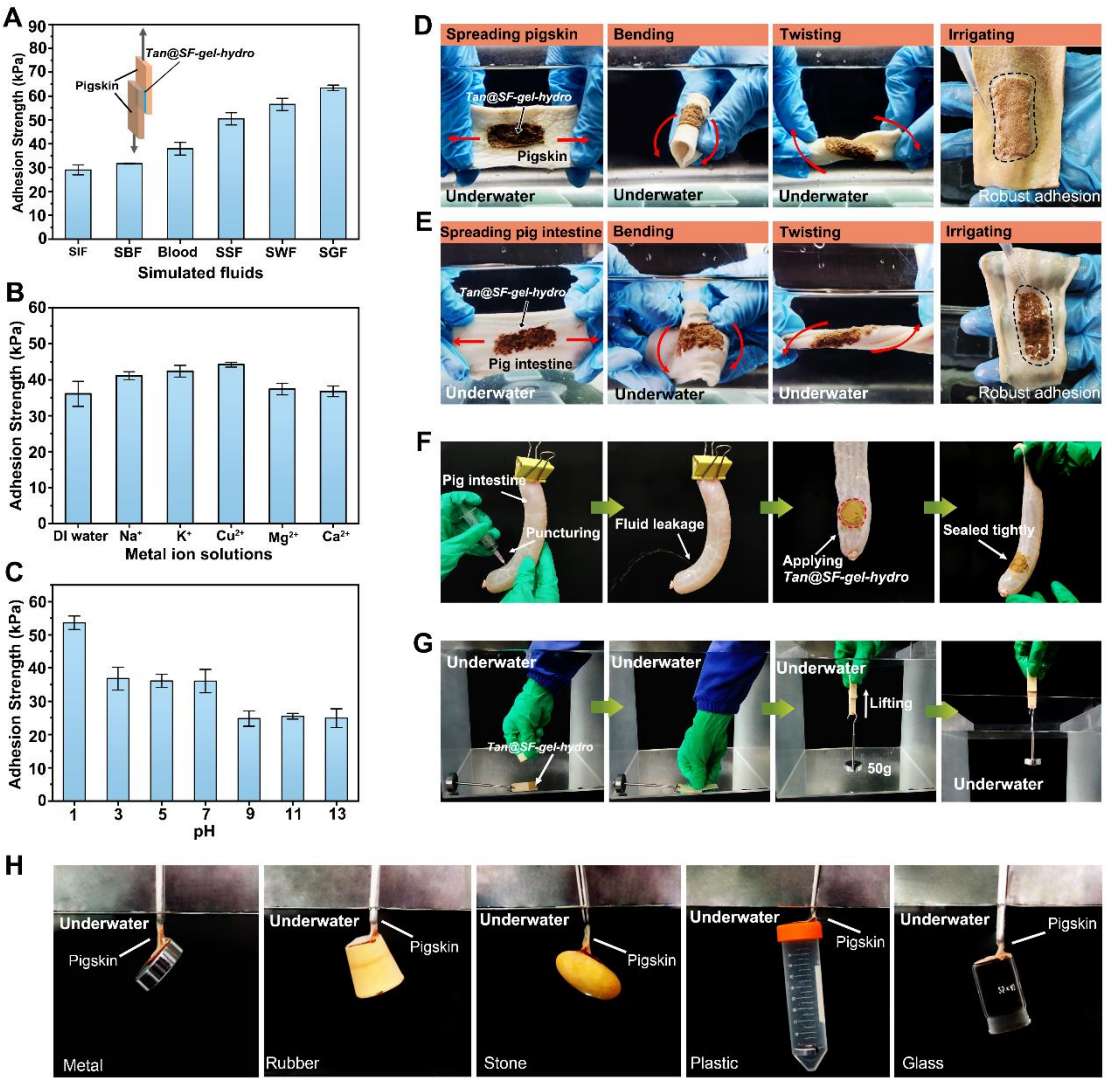

Figure 5. Adhesion strength of *Tan@SF-gel-hydro* in different liquids: A) simulated fluids, B) metal ion solutions, and C) aqueous solutions with different pH. Adhesive stability of *Tan@SF-gel-hydro* to D) pigskin and E) small intestine in water. F) Sealing of damaged intestine with *Tan@SF-gel-hydro*. G) Underwater adhesion between two pigskins with *Tan@SF-gel-hydro*. H) Adhesion stability of *Tan@SF-gel-hydro* to various substrates in water.

Figure 5B demonstrates the adhesion strength of *Tan@SF-gel-hydro* in various electrolyte solutions. The adhesion strength varied from 36.8 to 44.1 kPa without significant change, indicating that the type of electrolytes rarely affected adhesion strength. Comparing to adhesion strength in DI water (36.1 kPa), the adhesion strength in electrolyte solution was marginally increased, which may be attributed to the increased mechanical strength of *Tan@SF-gel-hydro* caused by the conformational shift of SF in electrolyte solutions (from random coil and α-helix to β-sheet) [51], and the metal chelation with *Tan@SF-gel-hydro* caused by the steric hindrance of the aromatic ring in TA and the electron donation/acceptance interaction between adjacent polyphenolic groups [52]. Consequently, it was possible for *Tan@SF-gel-hydro* to exhibit potent wet adhesive capabilities in electrolyte solutions.

Figure 5C depicts the adhesive strength under various pH conditions. The strongest adhesive strength, which was up to 53.6 ± 2.0 kPa, was observed at pH 1. This was due to the fact that the pyrogallol groups of TA were protonated and turned into excellent hydrogen donors in acidic circumstances, making them readily interactable with SF. The acid-resistance of SF, which allowed it to keep its mechanical characteristics and structural integrity in acidic environment, could also explain the enhanced adhesive strength under acidic conditions. The greater adhesion under acidic circumstances could also adequately explain why *Tan@SF-gel-hydro* exhibited excellent adhesion in the SGF group (Figure 5A). It was discovered that adhesive strength decreased as pH

increased. Due to the oxidation of polyphenol groups to quinone in alkaline conditions [52], the alkaline environment had led to the formation of an unstable polymer complex. Therefore, the wet adhesive strength of *Tan@SF-gel-hydro* was reduced in alkaline conditions compared to acidic and neutral conditions. Further, hydrolysis of SF under alkaline circumstances diminished the mechanical properties of *Tan@SF-gel-hydro*, resulting in decreased overall adhesive strength. The pH-dependent adhesiveness of *Tan@SF-gel-hydro* could pave the way for *Tan@SF-pwd-hydro* to be used in stomach hemostasis.

3.5 Adhesion stability and underwater adhesiveness

To demonstrate the practical application of *Tan@SF-gel-hydro*, the stability of adhesiveness in water was investigated utilizing a variety of inorganic materials and animal tissues as substrates. In water, *Tan@SF-gel-hydro* adhered firmly and stably to a variety of tissues. Not only did *Tan@SF-gel-hydro* adhere strongly to the pigskin, intestine, and kidney while submerged in water, but it also adhered stably to the tissues when it was bent and twisted (Figure 5D, Figure 5E and Figure S2A). In addition, even when irrigated with water, *Tan@SF-gel-hydro* did not detach from the organ (Figure S2B, Movie S2, Movie S3 and Movie S4). Adhering *Tan@SF-gel-hydro* to pigskin and intestine and then immersing them in water for 6 h made no differences in the adhesion effect (Figure S2C and Figure S2D). This demonstrated that the adhesion of *Tan@SF-gel-hydro* to tissues under water was long-lasting. In addition, Figure 5H demonstrates

that *Tan@SF-gel-hydro* maintains adhesion to a variety of inorganic surfaces underwater, such as metal, rubber, stone, plastic and glass.

As good sealing performance was beneficial for hemostasis of bleeding tissue, the sealing performance of *Tan@SF-gel-hydro* was evaluated using a damaged intestine. When PBS was injected into the intestine after its injured section was blocked with *Tan@SF-pwd-hydro*, no liquid leaking was observed(Figure 5F and Movie S5). This was due to the fact that *Tan@SF-pwd-hydro* absorbed liquids present on the intestine and subsequently created *Tan@SF-gel-hydro* to seal the injury. This phenomenon demonstrated the promising potential of *Tan@SF-gel-hydro* as an alternative to normal hand-sewn closure for avoiding leakage from damaged gastrointestinal organs [53].

The underwater adhesiveness of *Tan@SF-gel-hydro* was also evaluated. Two pieces of skin were bonded together with *Tan@SF-gel-hydro* underwater. They were then pulled out of the water while being subjected to a load of 50 g. Notably, the two bonded pigskins did not detach from each other during dynamic movement (Figure 5G and Movie S6), showing the strong adhesion and adhesive durability of *Tan@SF-gel-hydro* underwater. This could be explained as follows: When applied to wet surfaces, *Tan@SF-pwd-hydro* rapidly absorbed interfacial water and generated physically cross-linked *Tan@SF-gel-hydro* in situ due to its exceptional hydraulic conductivity. When *Tan@SF-gel-hydro* was effectively generated, the phenolic hydroxyl group of TA and

the carboxyl group of SF immediately attached to the amino group of the tissue, causing the gel to cling firmly to the tissue. The improved cohesion was also crucial for the outstanding wet adhesion capabilities *of Tan@SF-gel-hydro*. In summary, the bonding potentials of phenolic hydroxyl and carboxyl groups from *Tan@SF-gel-hydro* to amino groups in the tissue and the cohesion of *Tan@SF-gel-hydro* jointly contributed to the strong adhesive properties of *Tan@SF-gel-hydro*.

3.6 Biocompatibility Assessment

To reduce inflammation and other issues, biomaterials utilized in the body should be biodegradable. The in vivo biocompatibility of *Tan@SF-pwd-hydro* was evaluated in a New Zealand rabbit subcutaneous implantation model (Figure 6A). Figure 6B demonstrates that *Tan@SF-pwd-hydro* induced mild inflammation with little festering in the first 2 weeks after implantation; in contrast, Celox™ caused more severe inflammations with pustules and festering. *Tan@SF-pwd-hydro* degraded steadily over time and was fully degraded after 12 weeks, according to histological investigation (Figure 6B); nevertheless, Celox™ was still identifiable after 16 weeks. In conclusion, the biodegradability of *Tan@SF-pwd-hydro* was superior to that of Celox™.

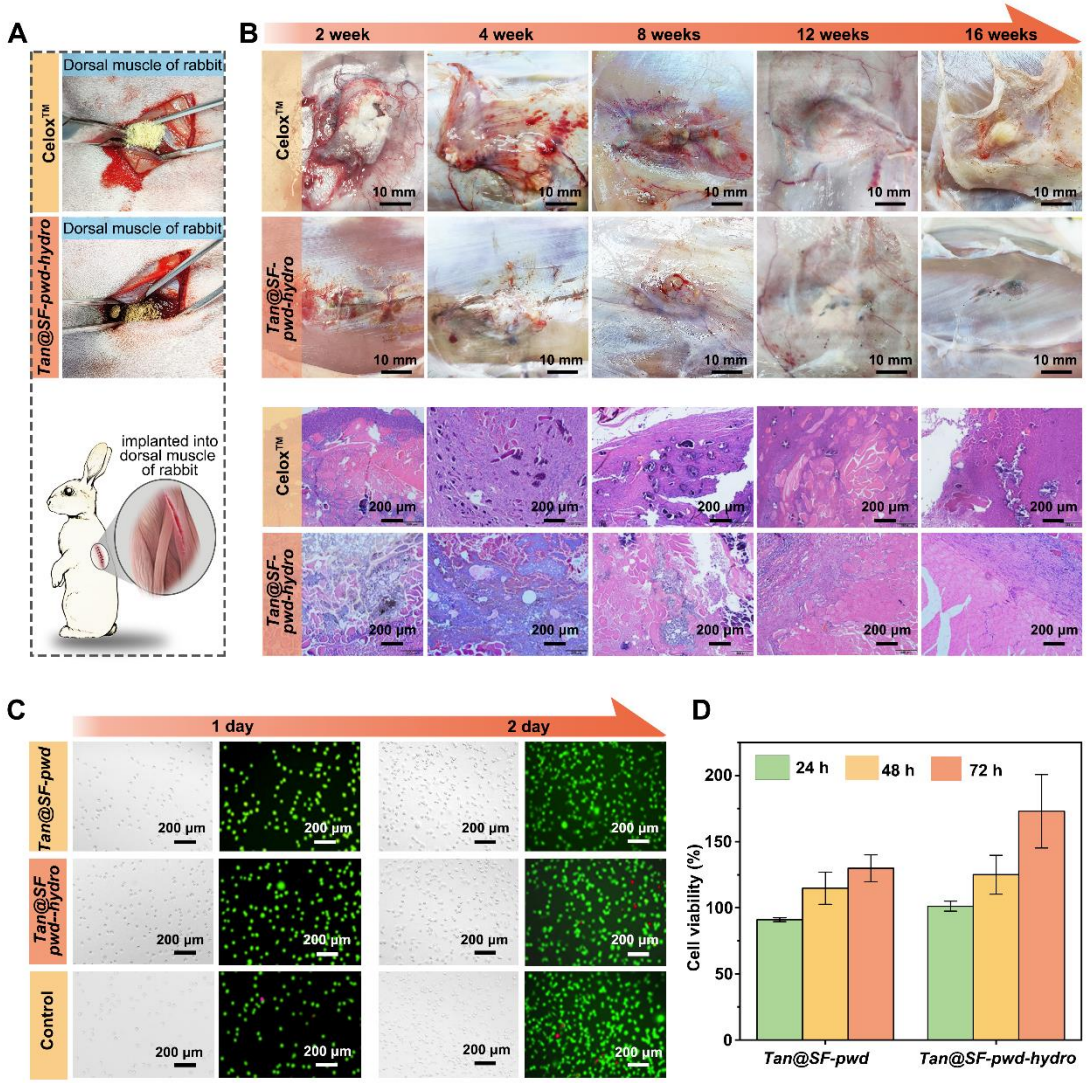

Figure 6. A) *In vivo* biodegradation models. B) Images and histological sections of the implantation sites. C) Live/dead cell double staining assay (green represents live cells, and red represents dead cells). D) Cell viability.

In the live/dead double staining experiment, all groups exhibited a significant green fluorescence signal corresponding to living cells. The living cells (green signal) for *Tan@SF-pwd-hydro* were round in shape on Day 1 and multiplied steadily on Day 2; very few dead cells (red signal) were observed in all groups (Figure 6C). In order to

further assess cytotoxicity, L929 cells were co-incubated with *Tan@SF-pwd-hydro* and *Tan@SF-pwd*. On Day 1, cell viability was greater than 80% in all groups, showing that the materials were generally non-toxic. On Day 2, cell viability was greater than 100% in the *Tan@SF-pwd-hydro* and *Tan@SF-pwd* groups (Figure 6D). These results revealed that *Tan@SF-pwd-hydro* and *Tan@SF-pwd* were not cytotoxic and could be utilized as hemostats without risk.

Good hemocompatibility contributes to the enhancement of the hemostatic and wound healing properties of hemostatic materials [54]. As shown in Figure 7A, the hemolysis rates of all samples were less than 5%, indicating that all materials exhibited acceptable hemocompatibility [55]. In comparison to SF and TA, the hemolysis rates of *Tan@SF-pwd* and *Tan@SF-pwd-hydro* were much lower, demonstrating their superior hemocompatibility. The hemolysis rate assay revealed that *Tan@SF-pwd* and *Tan@SF-pwd-hydro* were both exceptional candidates for use as secure biomaterials.

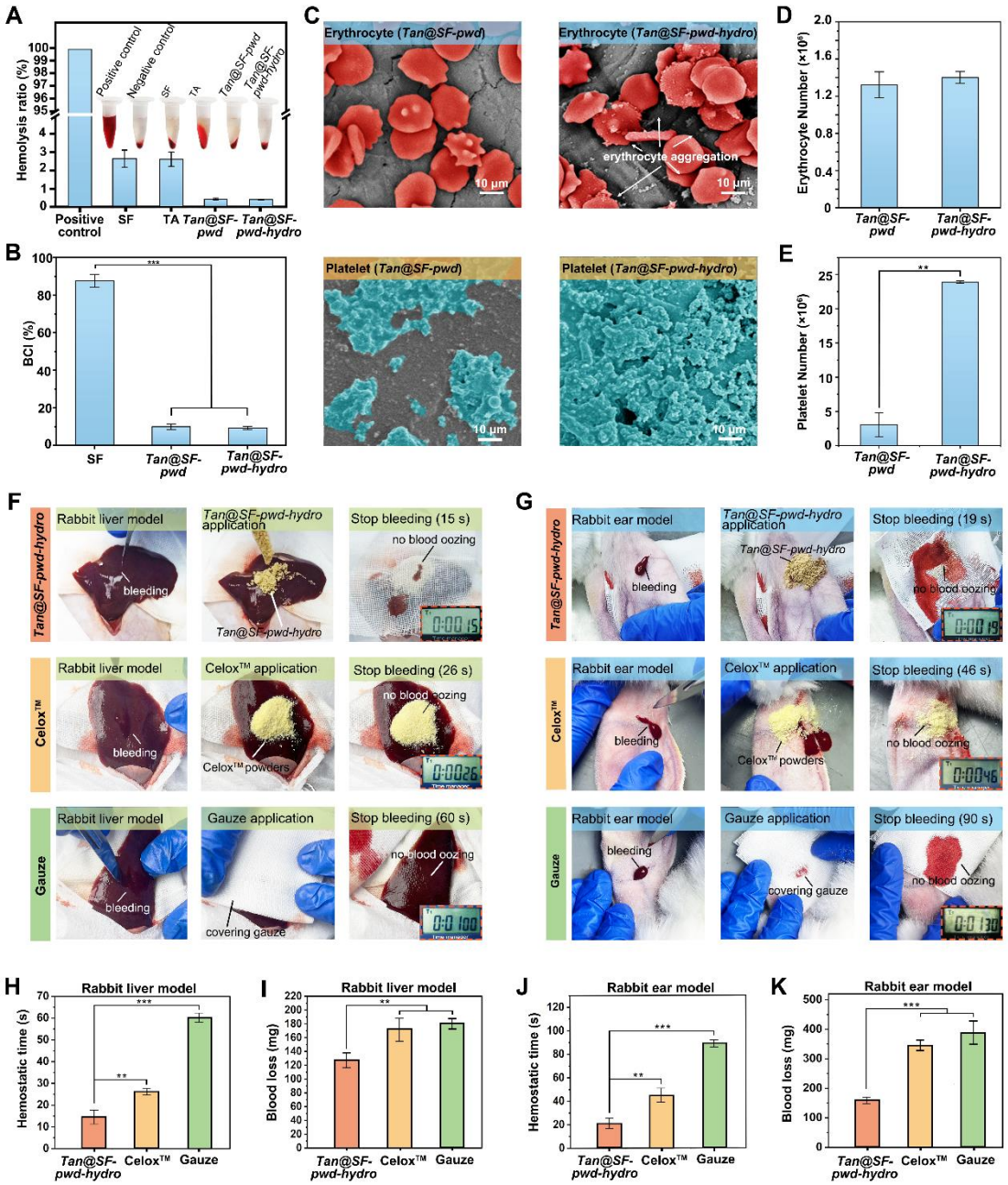

Figure 7. A) Hemolysis rate of various materials. B) BCI of various materials. C) SEM images of erythrocytes and platelets adhered to *Tan@SF-gel* and *Tan@SF-gel-hydro*. D) The number of erythrocytes adhered to *Tan@SF-pwd-hydro*. E) The number of platelets adhered to *Tan@SF-pwd-hydro*. Hemostatic performance of *Tan@SF-pwd-hydro*: F) liver model and G) ear artery model. Hemostatic time and blood loss of *Tan@SF-pwd-hydro*: H) Liver hemostatic time, I) Liver blood loss, J) Ear hemostatic

time, and K) Ear blood loss.

3.7 BCI and Adhesion of Erythrocyte and Platelet

BCI is typically used to characterize the blood coagulation capability of a substance. The coagulation rate decreases with increasing BCI. Figure 7B shows the BCI of SF, *Tan@SF-pwd*, and *Tan@SF-pwd-hydro*. The BCI of SF was as high as 87.7 ± 3.4%. However, the BCI of *Tan@SF-pwd* was only 9.9 ± 1.5%, indicating that *Tan@SF-pwd-hydro* generated a more rapid coagulation. In addition, *Tan@SF-pwd-hydro*, which was produced by doping PEG with *Tan@SF-pwd*, had the lowest BCI (9.3 ± 0.9%), indicating that the inclusion of PEG had no effect on the coagulation capacity.

Effective hemostats should rapidly absorb significant amounts of blood to concentrate coagulation components and create sturdy physical barriers with erythrocytes and platelets to achieve hemostasis [56]. Thus, the adhesion state of erythrocytes and platelets caused by hemostats is regularly checked to evaluate the hemostatic performance. The morphology of erythrocytes and platelets adhering to the surface of *Tan@SF-gel* and *Tan@SF-gel-hydro* were displayed in Figure 7C. Numerous erythrocytes and platelets adhered to the surface of *Tan@SF-gel-hydro* as a result of its powerful tissue adhesion property. Only a small percentage of erythrocytes denatured, indicating that *Tan@SF-gel-hydro* would not impair the normal physiological properties of erythrocytes [55]. Similar to erythrocytes, numerous platelets gathered on the surface as well (Figure 7C).

These results suggested that *Tan@SF-gel-hydro* could capture erythrocytes and platelets in plasma to form blood clots for fast hemostasis when applied to bleeding tissues [57].

Figures 7D and 7E depict the number of erythrocytes and platelets attached to *Tan@SF-gel-hydro*. Compared to *Tan@SF-gel*, the amount of adherent erythrocytes on *Tan@SF-gel-hydro* was somewhat greater (1.4×10^6) and the amount of adhering platelets was approximately 24×10^8. The exceptional erythrocyte and platelet aggregation and adhesion of *Tan@SF-gel* and *Tan@SF-gel-hydro* could be attributable to the following two factors. Blood proteins would establish hydrogen bonds with the polyphenolic groups of TA in *Tan@SF-gel* and *Tan@SF-gel-hydro*. Additionally, when chelation occurs between TA and blood metal ions (such as Fe^{2+} and Ca^{2+}), the chelation complex could aggregate countless erythrocytes and platelets to hasten hemostasis. Although both *Tan@SF-gel* and *Tan@SF-gel-hydro* adsorbed blood to aggregate erythrocytes and platelets for hemostasis, the coagulation rate of *Tan@SF-gel-hydro* was higher than that of *Tan@SF-gel*. This may be because polyethylene glycol (PEG) in *Tan@SF-pwd-hydro* granules greatly increased the hydrophilicity of *Tan@SF-pwd-hydro* (Figure 2C), hence accelerating the blood adsorption by *Tan@SF-pwd-hydro*. The increased blood adsorption facilitated extensive contact between *Tan@SF-pwd-hydro* and blood, which promoted the aggregation of erythrocytes and platelets in blood for enhanced coagulation.

3.8 *In vivo* Hemostasis

The vivo hemostatic capability was initially evaluated using liver hemorrhage models (Figure 7F). When thirsty *Tan@SF-pwd-hydro* or *Tan@SF-pwd* granules were applied to bleeding wounds, no additional removal of surface blood was required. *Tan@SF-pwd-hydro* offered a significant advantage in terms of reducing the hemostatic time. The hemostatic time of Celox ™, a commercial product, was as high as 26.8 ± 0.7 s, but the hemostatic time of *Tan@SF-pwd-hydro* was almost half of that of Celox ™ (Figure 7H). In addition, *Tan@SF-pwd-hydro* also reduced blood loss during bleeding. The blood loss of *Tan@SF-pwd-hydro* was 75% of that of Celox ™ (Figure 7I). In addition to the liver bleeding model, superior performance of *Tan@SF-pwd-hydro* was reported in the ear artery model as compared to Celox ™ (Figure 7G). The hemostatic time of *Tan@SF-pwd-hydro* was half of that of Celox ™ (Figure 7J), and the blood loss was less than half of that of Celox ™ (Figure 7K).

Through the development of liver and ear arterial hemorrhage models, *Tan@SF-pwd-hydro* demonstrated superior hemostatic properties to Celox ™. When *Tan@SF-pwd-hydro* converted to *Tan@SF-gel-hydro* upon contact with blood in a bleeding wound, a large number of polyphenolic groups provided by TA and carboxyl groups provided by SF interacted with amino groups from tissue, forming strong hydrogen bonds to reinforce adhesiveness, thereby facilitating sealing of the bleeding tissue toward

hemostasis.

3.9 *In vivo* Wound Healing

Wound healing after hemostasis remains one of the major healthcare problems globally [58]. The use of extra wound dressings following hemostasis may impede the healing process and perhaps increase the risk of infection. Thus, a dual-functional dressing that is capable of both hemostasis and wound healing is required. To verify the bifunctionality of *Tan@SF-pwd-hydro*, a rabbit model with a full skin defect was employed to investigate the ability of *Tan@SF-pwd-hydro* to promote wound healing in addition to its hemostatic properties. Similarly, while applying the thirsty *Tan@SF-pwd-hydro* or *Tan@SF-pwd* granules, no further blood or exudate removal was conducted over wounds.

All groups of materials were shown to have a wound-healing-promoting impact, however the *Tan@SF-pwd-hydro* group had the most rapid wound healing (Figure 8A and Figure B). In contrast to the commercial product Tegaderm ™, *Tan@SF-pwd-hydro* in its thirsty granular state quickly absorbed blood or bodily fluids from the wound area to create *Tan@SF-gel-hydro*, which assisted in tissue repair. On Day 15 postoperatively, the wound treated with Tegaderm ™ still had substantial crusting, whereas the wound treated with *Tan@SF-pwd-hydro* was nearly healed and had a 96.4% healing rate (Figure 8C). It could be inferred that *Tan@SF-pwd-hydro* displayed a substantial ability

for wound repair, which could be due to the increased antioxidant and antibacterial activity of TA in *Tan@SF-pwd-hydro* [59] and the role of SF as an active biomaterial in the process of wound healing [60].

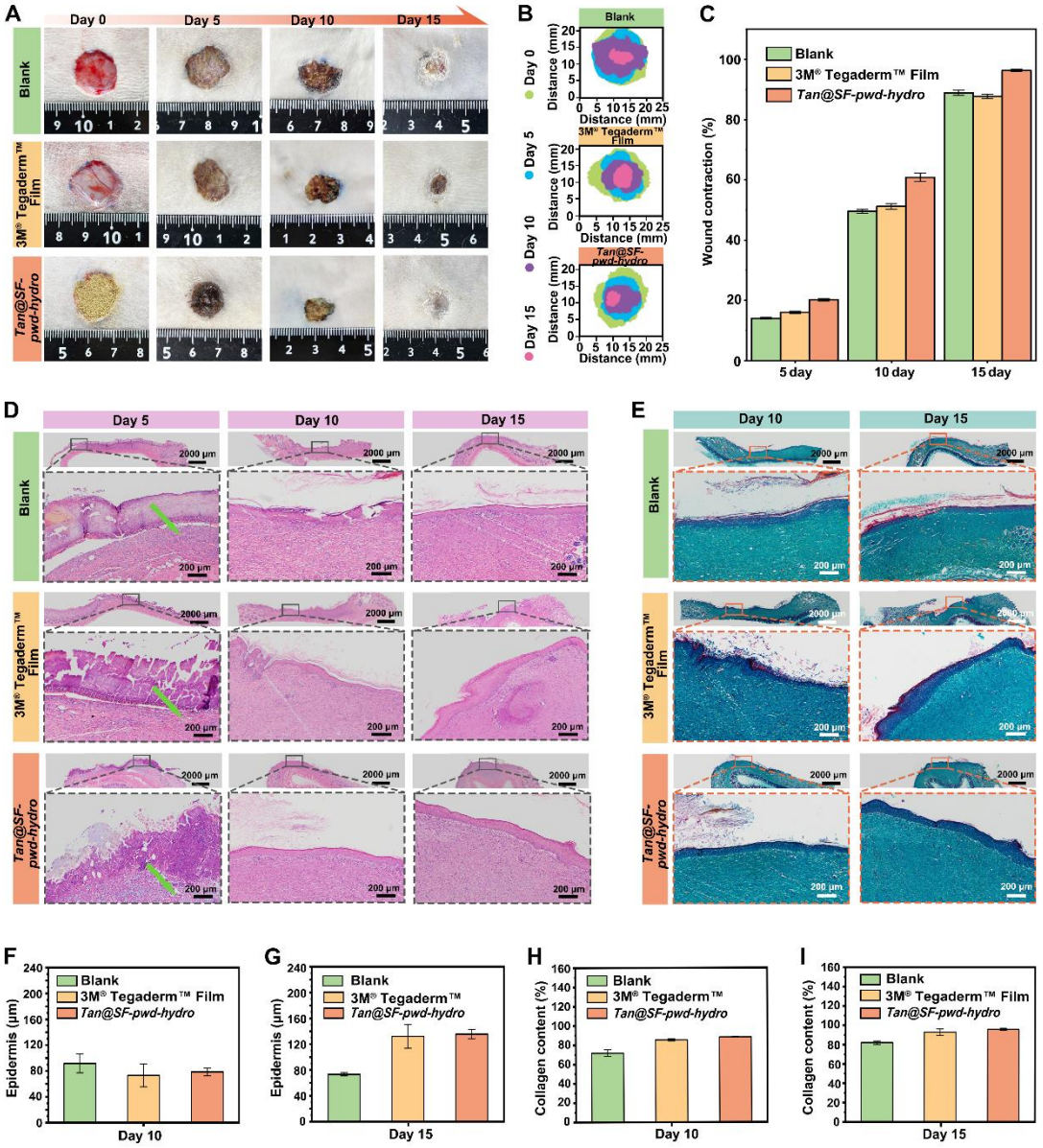

Figure 8. A) Images of wounds during healing. B) Traces of the wound area. C) Wound contraction percentage. D) H&E-stained histological sections of wound tissues (green arrows indicate inflammatory cells). E) Masson-stained histological sections of wound

tissues. Thickness of epidermis on F) Day 10 and G) Day 15. Collagen content on H) Day 10 and I) Day 15.

Histological investigation (H&E and Masson staining) was also conducted to further evaluate the pro-healing impact of *Tan@SF-pwd-hydro*. As demonstrated in Figure 8D, an inflammatory reaction emerged on Day 5, however on Day 10 there were no substantial inflammatory responses in the *Tan@SF-pwd-hydro* group. In addition, little granulation tissue was found on Day 5 in the *Tan@SF-pwd-hydro* and Tegaderm ™ groups, demonstrating that *Tan@SF-pwd-hydro* did not induce any rejection reaction and expedited wound healing. On Day 15, the mature granulation tissue was replaced by collagen and the epithelial structures were restored in all three groups, but crusting was still present (Figure 8D and Figure 8E).

The thickness of the epidermis may indicate the influence of dressing materials on wound healing. On Day 10, the epidermal thicknesses of the three groups were equal; however, on Day 15, the *Tan@SF-pwd-hydro* and Tegaderm ™ groups had much thicker epidermis than the blank group. As the epidermis of the *Tan@SF-pwd-hydro* group was more uniform than that of the Tegaderm ™ group, it could be extrapolated that *Tan@SF-pwd-hydro* showed superior tissue healing capacity (Figure 8F and Figure 8G).

Collagen is an essential component of skin, hence collagen deposition is one of the most significant indications of wound healing [61]. The bigger the collagen content is, the more effective the wound healing is. In this study, subcutaneous collagen contents was detected by Masson staining (Figure 8E). On day 10, the collagen content of *Tan@SF-pwd-hydro* was 88.3 ± 0.5% and that of the Tegaderm ™ group was 85.4 ± 1.1%, both significantly higher than the blank group (Figure 8H); the *Tan@SF-pwd-hydro* group and the Tegaderm ™ group also showed better wound healing. As demonstrated in Figure 8I, the collagen content of the *Tan@SF-pwd-hydro* group on Day 15 was 95.8±1.1%, whereas that of the Tegaderm ™ group was 92.2 ± 3.4%. This showed that the *Tan@SF-pwd-hydro* group healed much better than the Tegaderm ™ and control groups, dramatically accelerating wound healing to reduce healing time. These findings suggested that *Tan@SF-pwd-hydro* was a dual-functional dressing that could continue to promote wound healing after achieving hemostasis.

4 CONCLUSIONS

Bioadhesives have been utilized extensively for hemostasis and tissue healing. However, the presence of biofluids, such as blood and exudate, over the wound has a detrimental effect on the potential and durability of the adhesiveness, resulting in the failure of hemostasis and deficient wound healing. This study produced a hydro-stimulated thirsty polyphenolic silk granule, *Tan@SF-pwd-hydro*, that shielded wetness over wound by adsorption of biofluids to form *Tan@SF-gel-hydro in situ*, a bioadhesive dressing, in

order to achieve strong and stable wet-adhesion. *Tan@SF-pwd-hydro* was found to have a peak adhesive strength of 59.8 ± 2.1 kPa and the ability to maintain adhesiveness in a variety of severe conditions. When used as hemostat, the hemostatic time of *Tan@SF-pwd-hydro* in the liver bleeding model was 14.8 ± 5.2 s, which was only about half of that of the commercial hemostatic product, Celox ™. Furthermore, the healing time of *Tan@SF-pwd-hydro* in the full-thickness skin defect model was 15 days, which was shorter than that of the commercial adhesive wound dressing product, Tegaderm ™. In addition, *Tan@SF-pwd-hydro* had no cytotoxic effects on L929 cells or RBCs, and it was completely biodegradable in the subcutaneous muscle implantation model. Due to these benefits, *Tan@SF-pwd-hydro* has tremendous potential as an effective and safe bioadhesive dressing for hemostasis and tissue healing, and consequently for therapeutic applications. This pioneering study utilized the adverse wetness over wounds to arouse robust adhesiveness by converting thirsty granules to bioadhesives *in situ* for wound care, creatively turning adversity into opportunities. Moreover, this study offered a new, simple and clean technique for making biomaterials with reduced carbon footprint.

ASSOCIATED CONTENT

Supporting Information

The following files are available free of charge. Effect of TA concentration on adhesiveness; Adhesive stability of *Tan@SF-gel-hydro* on various tissues (PDF).

Preparation of *Tan@SF-pwd-hydro* (Movie S1, MP4); Water irrigated *Tan@SF-gel-hydro* adhering to pig kidney (Movie S2, MP4); Water irrigated *Tan@SF-gel-hydro* adhering to pig liver (Movie S3, MP4); Water irrigated *Tan@SF-gel-hydro* adhering to pig heart (Movie S4, MP4); *Tan@SF-pwd-hydro* sealed the damaged intestines (Movie S5, MP4); The underwater adhesiveness of *Tan@SF-gel-hydro* (Movie S6, MP4).

ACKNOWLEDGEMENTS

This work was supported by the Natural Science Foundation of Chongqing, China (cstb2022nscq-msx0555) and the National Natural Science Foundation of China (No. 52103096).

DECLARATION OF INTERESTS

There are no conflicts of interest to declare.

CRediT authorship contribution statement

All authors participated in drafting the article and critically revised important content, and endorsed the final version. **Li Xiong:** Methodology, Data Curation, Formal Analysis, Investigation and Writing-original draft. **Huan Wang:** Methodology, Data Curation, Formal Analysis and Investigation. **Junsu Wang:** Visualization and Validation. **Jinyang Luo:** Methodology. **Ruiqi Xie, Fei Lu** and **Guangqian Lan**: Conceptualization and Resources. **Liang Ju Ning, Rong Yin** and **Wenyi Wang:**

Supervision and Validation. **Enling Hu:** Project Administration, Supervision and Writing-review & editing.

REFERENCE

(1) Huang, Y.; Zhao, X.; Zhang, Z.; Liang, Y.; Yin, Z.; Chen, B.; Bai, L.; Han, Y.; Guo, B. Degradable Gelatin-Based IPN Cryogel Hemostat for Rapidly Stopping Deep Noncompressible Hemorrhage and Simultaneously Improving Wound Healing. *Chemistry of Materials* **2020**, *32* (15), 6595-6610. DOI: 10.1021/acs.chemmater.0c02030.

(2) Li, Q.; Hu, E.; Yu, K.; Xie, R.; Lu, F.; Lu, B.; Bao, R.; Zhao, T.; Dai, F.; Lan, G. Self-Propelling Janus Particles for Hemostasis in Perforating and Irregular Wounds with Massive Hemorrhage. *Advanced Functional Materials* **2020**, *30* (42), 2004153. DOI: https://doi.org/10.1002/adfm.202004153.

(3) Zhao, X.; Guo, B.; Wu, H.; Liang, Y.; Ma, P. X. Injectable Antibacterial Conductive Nanocomposite Cryogels with Rapid Shape Recovery for Noncompressible Hemorrhage and Wound Healing. *Nature Communications* **2018**, *9* (1), 2784. DOI: 10.1038/s41467-018-04998-9.

(4) Yu, L.; Zhang, H.; Xiao, L.; Fan, J.; Li, T. A Bio-Inorganic Hybrid Hemostatic Gauze for Effective Control of Fatal Emergency Hemorrhage in "Platinum Ten Minutes". *ACS Applied Materials & Interfaces* **2022**, *14* (19), 21814-21821. DOI: 10.1021/acsami.1c24668.

(5) Li, X.-F.; Lu, P.; Jia, H.-R.; Li, G.; Zhu, B.; Wang, X.; Wu, F.-G. Emerging Materials for Hemostasis. *Coordination Chemistry Reviews* **2023**, *475*, 214823. DOI: https://doi.org/10.1016/j.ccr.2022.214823.

(6) Liang, Y.; Li, Z.; Huang, Y.; Yu, R.; Guo, B. Dual-Dynamic-Bond Cross-Linked Antibacterial Adhesive Hydrogel Sealants with on-Demand Removability for Post-Wound-Closure and Infected Wound Healing. *ACS Nano* **2021**, *15* (4), 7078-7093. DOI: 10.1021/acsnano.1c00204.

(7) Lv, C.; Li, L.; Jiao, Z.; Yan, H.; Wang, Z.; Wu, Z.; Guo, M.; Wang, Y.; Zhang, P. Improved Hemostatic Effects by Fe3+ Modified Biomimetic PLLA Cotton-Like Mat via Sodium Alginate Grafted with Dopamine. *Bioactive Materials* **2021**, *6* (8), 2346-2359. DOI: https://doi.org/10.1016/j.bioactmat.2021.01.002.

(8) Wang, P.; Pu, Y.; Ren, Y.; Liu, S.; Yang, R.; Tan, X.; Zhang, W.; Shi, T.; Li, S.; Chi, B. Bio-inspired Hydrogel-Based Bandage with Robust Adhesive and Antibacterial Abilities for Skin Closure. *Science China Materials* **2022**, *65* (1), 246-254. DOI: 10.1007/s40843-021-1724-8.

(9) Freedman, B. R.; Hwang, C.; Talbot, S.; Hibler, B.; Matoori, S.; Mooney, D. J. Breakthrough Treatments for Accelerated Wound Healing. *Science Advances* **2023**, *9* (20), eade7007. DOI: doi:10.1126/sciadv.ade7007.

(10) Montazerian, H.; Davoodi, E.; Baidya, A.; Baghdasarian, S.; Sarikhani, E.; Meyer, C. E.; Haghniaz, R.; Badv, M.; Annabi, N.; Khademhosseini, A.; et al. Engineered Hemostatic Biomaterials for Sealing Wounds. *Chemical Reviews* **2022**, *122* (15), 12864-12903. DOI: 10.1021/acs.chemrev.1c01015.

(11) Ma, C.; Sun, J.; Li, B.; Feng, Y.; Sun, Y.; Xiang, L.; Wu, B.; Xiao, L.; Liu, B.; Petrovskii, V. S.; et al. Ultra-strong Bio-glue from Genetically Engineered Polypeptides. *Nature Communications* **2021**, *12* (1), 3613. DOI: 10.1038/s41467-021-23117-9.

(12) Kim, S. H.; Lee, Y. J.; Chao, J. R.; Kim, D. Y.; Sultan, M. T.; Lee, H. J.; Lee, J. M.; Lee, J. S.; Lee, O. J.;

Hong, H.; et al. Rapidly Photocurable Silk Fibroin Sealant for Clinical Applications. *NPG Asia Materials* **2020**, *12* (1), 46. DOI: 10.1038/s41427-020-0227-6.
(13) Liang, Y.; Xu, H.; Li, Z.; Zhangji, A.; Guo, B. Bioinspired Injectable Self-Healing Hydrogel Sealant with Fault-Tolerant and Repeated Thermo-Responsive Adhesion for Sutureless Post-Wound-Closure and Wound Healing. *Nano-Micro Letters* **2022**, *14* (1), 185. DOI: 10.1007/s40820-022-00928-z.
(14) Zhang, W.; Wang, R.; Sun, Z.; Zhu, X.; Zhao, Q.; Zhang, T.; Cholewinski, A.; Yang, F.; Zhao, B.; Pinnaratip, R.; et al. Catechol-functionalized Hydrogels: Biomimetic Design, Adhesion Mechanism, and Biomedical Applications. *Chemical Society Reviews* **2020**, *49* (2), 433-464, 10.1039/C9CS00285E. DOI: 10.1039/C9CS00285E.
(15) Kumar, A.; Domb, A. J. Polymerization Enhancers for Cyanoacrylate Skin Adhesive. *Macromolecular Bioscience* **2021**, *21* (10), 2100143. DOI: https://doi.org/10.1002/mabi.202100143.
(16) Teng, L.; Shao, Z.; Bai, Q.; Zhang, X.; He, Y.-S.; Lu, J.; Zou, D.; Feng, C.; Dong, C.-M. Biomimetic Glycopolypeptide Hydrogels with Tunable Adhesion and Microporous Structure for Fast Hemostasis and Highly Efficient Wound Healing. *Advanced Functional Materials* **2021**, *31* (43), 2105628. DOI: https://doi.org/10.1002/adfm.202105628.
(17) Spring, M. A. Use of a Lysine-Derived Urethane Surgical Adhesive as an Alternative to Progressive Tension Sutures in Abdominoplasty Patients: A Cohort Study. *Aesthetic Surgery Journal* **2018**, *38* (12), 1318-1329. DOI: 10.1093/asj/sjy094 (acccessed 6/5/2023).
(18) Nam, S.; Mooney, D. Polymeric Tissue Adhesives. *Chemical Reviews* **2021**, *121* (18), 11336-11384. DOI: 10.1021/acs.chemrev.0c00798.
(19) Qiu, H.; Lan, G.; Ding, W.; Wang, X.; Wang, W.; Shou, D.; Lu, F.; Hu, E.; Yu, K.; Shang, S.; et al. Dual-Driven Hemostats Featured with Puncturing Erythrocytes for Severe Bleeding in Complex Wounds. *Research* **2022**, *2022*. DOI: doi:10.34133/2022/9762746.
(20) Sahoo, J. K.; Hasturk, O.; Falcucci, T.; Kaplan, D. L. Silk Chemistry and Biomedical Material Designs. *Nature Reviews Chemistry* **2023**, *7* (5), 302-318. DOI: 10.1038/s41570-023-00486-x.
(21) Liu, J.; Shi, L.; Deng, Y.; Zou, M.; Cai, B.; Song, Y.; Wang, Z.; Wang, L. Silk Sericin-Based Materials for Biomedical Applications. *Biomaterials* **2022**, *287*, 121638. DOI: https://doi.org/10.1016/j.biomaterials.2022.121638.
(22) Yang, Z.; Fan, S.; Ma, W.; Li, Z.; Ren, X. Flexible adhesive GelMA/SF-based Patch Embedded with Polydopamine N-Halamine Nanoparticles for Repair of Infected Wounds. *Chemical Engineering Journal* **2023**, *460*, 141732. DOI: https://doi.org/10.1016/j.cej.2023.141732.
(23) Osman, A.; Lin, E.; Hwang, D. S. A Sticky Carbohydrate Meets A Mussel Adhesive: Catechol-Conjugated Levan for Hemostatic and Wound Healing Applications. *Carbohydrate Polymers* **2023**, *299*, 120172. DOI: https://doi.org/10.1016/j.carbpol.2022.120172.
(24) Feng, W.; Wang, Z. Tailoring the Swelling-Shrinkable Behavior of Hydrogels for Biomedical Applications. *Advanced Science n/a* (n/a), 2303326. DOI: https://doi.org/10.1002/advs.202303326.
(25) Chen, R.; Mao, L.; Matindi, C. N.; Liu, G.; He, J.; Cui, Z.; Ma, X.; Fang, K.; Wu, B.; Mamba, B. B.; et al. Tailoring the Micro-structure of PVC/SMA-g-PEG Blend Ultrafiltration Membrane with Simultaneously Enhanced Hydrophilicity and Toughness by In Situ Reaction-Controlled Phase Inversion. *Journal of Membrane Science* **2022**, *653*, 120545. DOI: https://doi.org/10.1016/j.memsci.2022.120545.
(26) Shi, X.; Lei, Y.; Xue, W.; Liu, X.; Li, S.; Xu, Y.; Lv, C.; Wang, S.; Wang, J.; Yan, G. Drivers in Carbon Dioxide, Air Pollutants Emissions and Health Benefits of China's Clean Vehicle Fleet 2019–2035. *Journal of*

Cleaner Production **2023**, *391*, 136167. DOI: https://doi.org/10.1016/j.jclepro.2023.136167.
(27) Zhou, Z.; Xiao, J.; Guan, S.; Geng, Z.; Zhao, R.; Gao, B. A Hydrogen-Bonded Antibacterial Curdlan-Tannic Acid Hydrogel with An Antioxidant and Hemostatic Function for Wound Healing. *Carbohydrate Polymers* **2022**, *285*, 119235. DOI: https://doi.org/10.1016/j.carbpol.2022.119235.
(28) Li, Q.; Hu, E.; Yu, K.; Lu, M.; Xie, R.; Lu, F.; Lu, B.; Bao, R.; Lan, G. Magnetic Field-mediated Janus Particles with Sustained Driving Capability for Severe Bleeding Control in Perforating and Inflected Wounds. *Bioactive Materials* **2021**, *6* (12), 4625-4639. DOI: https://doi.org/10.1016/j.bioactmat.2021.05.006.
(29) Jiang, Q.; Luo, B.; Wu, Z.; Gu, B.; Xu, C.; Li, X.; Wang, X. Corn Stalk/AgNPs Modified Chitin Composite Hemostatic Sponge with High Absorbency, Rapid Shape Recovery and Promoting Wound Healing Ability. *Chemical Engineering Journal* **2021**, *421*, 129815. DOI: https://doi.org/10.1016/j.cej.2021.129815.
(30) Shi, Z.; Lan, G.; Hu, E.; Lu, F.; Qian, P.; Liu, J.; Dai, F.; Xie, R. Targeted Delivery of Hemostats to Complex Bleeding Wounds with Magnetic Guidance for Instant Hemostasis. *Chemical Engineering Journal* **2022**, *427*, 130916. DOI: https://doi.org/10.1016/j.cej.2021.130916.
(31) Li, Y.; Zhang, Y.; Wang, Y.; Yu, K.; Hu, E.; Lu, F.; Shang, S.; Xie, R.; Lan, G. Regulating Wound Moisture for Accelerated Healing: A Strategy for The Continuous Drainage of Wound Exudates by Mimicking Plant Transpiration. *Chemical Engineering Journal* **2022**, *429*, 131964. DOI: https://doi.org/10.1016/j.cej.2021.131964.
(32) Zhang, L.; Zhang, M.; Lu, J.; Tang, A.; Zhu, L. Highly Permeable Thin-Film Nanocomposite Membranes Embedded with PDA/PEG Nanocapsules as Water Transport Channels. *Journal of Membrane Science* **2019**, *586*, 115-121. DOI: https://doi.org/10.1016/j.memsci.2019.05.065.
(33) Ahmadian, Z.; Correia, A.; Hasany, M.; Figueiredo, P.; Dobakhti, F.; Eskandari, M. R.; Hosseini, S. H.; Abiri, R.; Khorshid, S.; Hirvonen, J.; et al. A Hydrogen-Bonded Extracellular Matrix-Mimicking Bactericidal Hydrogel with Radical Scavenging and Hemostatic Function for pH-Responsive Wound Healing Acceleration. *Advanced Healthcare Materials* **2021**, *10* (3), 2001122. DOI: https://doi.org/10.1002/adhm.202001122.
(34) Manchineella, S.; Thrivikraman, G.; Khanum, K. K.; Ramamurthy, P. C.; Basu, B.; Govindaraju, T. Pigmented Silk Nanofibrous Composite for Skeletal Muscle Tissue Engineering. *Advanced Healthcare Materials* **2016**, *5* (10), 1222-1232. DOI: https://doi.org/10.1002/adhm.201501066.
(35) Bai, S.; Zhang, X.; Cai, P.; Huang, X.; Huang, Y.; Liu, R.; Zhang, M.; Song, J.; Chen, X.; Yang, H. A Silk-based Sealant with Tough Adhesion for Instant Hemostasis of Bleeding Tissues. *Nanoscale Horizons* **2019**, *4* (6), 1333-1341, 10.1039/C9NH00317G. DOI: 10.1039/C9NH00317G.
(36) Gao, X.; Dai, Q.; Yao, L.; Dong, H.; Li, Q.; Cao, X. A Medical Adhesive Used in A Wet Environment by Blending Tannic Acid and Silk Fibroin. *Biomaterials Science* **2020**, *8* (9), 2694-2701, 10.1039/D0BM00322K. DOI: 10.1039/D0BM00322K.
(37) Chen, S.; Liu, S.; Zhang, L.; Han, Q.; Liu, H.; Shen, J.; Li, G.; Zhang, L.; Yang, Y. Construction of Injectable Silk Fibroin/Polydopamine Hydrogel for Treatment of Spinal Cord Injury. *Chemical Engineering Journal* **2020**, *399*, 125795. DOI: https://doi.org/10.1016/j.cej.2020.125795.
(38) Ren, X.; Ge, J.; Meng, X.; Qiu, X.; Ren, J.; Tang, F. Sensitive Detection of Dopamine and Quinone Drugs Based on The Quenching of The Fluorescence of Carbon Dots. *Science Bulletin* **2016**, *61* (20), 1615-1623. DOI: https://doi.org/10.1007/s11434-016-1172-1.
(39) Menapace, I.; Yiming, W.; Masad, E. Chemical Analysis of Surface and Bulk of Asphalt Binders Aged

with Accelerated Weathering Tester and Standard Aging Methods. *Fuel* **2017**, *202*, 366-379. DOI: https://doi.org/10.1016/j.fuel.2017.04.042.
(40) Dong, H.; Wang, L.; Du, L.; Wang, X.; Li, Q.; Wang, X.; Zhang, J.; Nie, J.; Ma, G. Smart Polycationic Hydrogel Dressing for Dynamic Wound Healing. *Small* **2022**, *18* (25), 2201620. DOI: https://doi.org/10.1002/smll.202201620.
(41) Chen, J.; He, J.; Yang, Y.; Qiao, L.; Hu, J.; Zhang, J.; Guo, B. Antibacterial Adhesive Self-Healing Hydrogels to Promote Diabetic Wound Healing. *Acta Biomaterialia* **2022**, *146*, 119-130. DOI: https://doi.org/10.1016/j.actbio.2022.04.041.
(42) Zheng, H.; Chen, M.; Sun, Y.; Zuo, B. Self-Healing, Wet-Adhesion Silk Fibroin Conductive Hydrogel as A Wearable Strain Sensor for Underwater Applications. *Chemical Engineering Journal* **2022**, *446*, 136931. DOI: https://doi.org/10.1016/j.cej.2022.136931.
(43) Feng, W.; Wang, Z. Shear-thinning and Self-Healing Chitosan-Graphene Oxide Hydrogel for Hemostasis and Wound Healing. *Carbohydrate Polymers* **2022**, *294*, 119824. DOI: https://doi.org/10.1016/j.carbpol.2022.119824.
(44) Han, L.; Liu, M.; Yan, B.; Li, Y.; Lan, J.; Shi, L.; Ran, R. Polydopamine/Polystyrene Nanocomposite Double-Layer Strain Sensor Hydrogel with Mechanical, Self-Healing, Adhesive and Conductive Properties. *Materials Science and Engineering: C* **2020**, *109*, 110567. DOI: https://doi.org/10.1016/j.msec.2019.110567.
(45) Wang, X.; Guo, Y.; Li, J.; You, M.; Yu, Y.; Yang, J.; Qin, G.; Chen, Q. Tough Wet Adhesion of Hydrogen-Bond-Based Hydrogel with On-Demand Debonding and Efficient Hemostasis. *ACS Applied Materials & Interfaces* **2022**, *14* (31), 36166-36177. DOI: 10.1021/acsami.2c10202.
(46) Fan, X.; Fang, Y.; Zhou, W.; Yan, L.; Xu, Y.; Zhu, H.; Liu, H. Mussel Foot Protein Inspired Tough Tissue-Selective Underwater Adhesive Hydrogel. *Materials Horizons* **2021**, *8* (3), 997-1007, 10.1039/D0MH01231A. DOI: 10.1039/D0MH01231A.
(47) Lei, K.; Wang, K.; Sun, Y.; Zheng, Z.; Wang, X. Rapid-Fabricated and Recoverable Dual-Network Hydrogel with Inherently Anti-Bacterial Abilities for Potential Adhesive Dressings. *Advanced Functional Materials* **2021**, *31* (6), 2008010. DOI: https://doi.org/10.1002/adfm.202008010.
(48) Palmer-Green, D.; Brownlow, M.; Hopkins, J.; Eley, J.; Jaques, R.; Hunter, G. Epidemiological Study of Injury and Illness in Great Britain Short-Track Speed Skating. *British Journal of Sports Medicine* **2014**, *48* (7), 649. DOI: 10.1136/bjsports-2014-093494.238.
(49) Nathanson, A.; Haynes, P.; Galanis, D. Surfing Injuries. *The American Journal of Emergency Medicine* **2002**, *20* (3), 155-160. DOI: https://doi.org/10.1053/ajem.2002.32650.
(50) Ma, X.; Zhou, X.; Ding, J.; Huang, B.; Wang, P.; Zhao, Y.; Mu, Q.; Zhang, S.; Ren, C.; Xu, W. Hydrogels for Underwater Adhesion: Adhesion Mechanism, Design Strategies and Applications. *Journal of Materials Chemistry A* **2022**, *10* (22), 11823-11853, 10.1039/D2TA01960D. DOI: 10.1039/D2TA01960D.
(51) Ruan, Q.-X.; Zhou, P. Sodium Ion Effect on Silk Fibroin Conformation Characterized by Solid-State NMR and Generalized 2D NMR–NMR Correlation. *Journal of Molecular Structure* **2008**, *883-884*, 85-90. DOI: https://doi.org/10.1016/j.molstruc.2007.11.055.
(52) Chen, C.; Yang, H.; Yang, X.; Ma, Q. Tannic Acid: A Crosslinker Leading to Versatile Functional Polymeric Networks: A Review. *RSC Advances* **2022**, *12* (13), 7689-7711, 10.1039/D1RA07657D. DOI: 10.1039/D1RA07657D.
(53) Wu, J.; Yuk, H.; Sarrafian, T. L.; Guo, C. F.; Griffiths, L. G.; Nabzdyk, C. S.; Zhao, X. An off-The-Shelf

Bioadhesive Patch for Sutureless Repair of Gastrointestinal Defects. *Science Translational Medicine* **2022**, *14* (630), eabh2857. DOI: doi:10.1126/scitranslmed.abh2857.

(54) Yang, E.; Hou, W.; Liu, K.; Yang, H.; Wei, W.; Kang, H.; Dai, H. A Multifunctional Chitosan Hydrogel Dressing for Liver Hemostasis and Infected Wound Healing. *Carbohydrate Polymers* **2022**, *291*, 119631. DOI: https://doi.org/10.1016/j.carbpol.2022.119631.

(55) Huang, Y.; Gu, B.; Salles-Crawley, I. I.; Taylor, K. A.; Yu, L.; Ren, J.; Liu, X.; Emerson, M.; Longstaff, C.; Hughes, A. D.; et al. Fibrinogen-mimicking, Multiarm Nanovesicles for Human Thrombus-Specific Delivery of Tissue Plasminogen Activator and Targeted Thrombolytic Therapy. *Science Advances* **2021**, *7* (23), eabf9033. DOI: doi:10.1126/sciadv.abf9033.

(56) Peng, X.; Xu, X.; Deng, Y.; Xie, X.; Xu, L.; Xu, X.; Yuan, W.; Yang, B.; Yang, X.; Xia, X.; et al. Ultrafast Self-Gelling and Wet Adhesive Powder for Acute Hemostasis and Wound Healing. *Advanced Functional Materials* **2021**, *31* (33), 2102583. DOI: https://doi.org/10.1002/adfm.202102583.

(57) He, H.; Zhou, W.; Gao, J.; Wang, F.; Wang, S.; Fang, Y.; Gao, Y.; Chen, W.; Zhang, W.; Weng, Y.; et al. Efficient, Biosafe and Tissue Adhesive Hemostatic Cotton Gauze with Controlled Balance of Hydrophilicity and Hydrophobicity. *Nature Communications* **2022**, *13* (1), 552. DOI: 10.1038/s41467-022-28209-8.

(58) Wang, Y.; Wang, Z.; Dong, Y. Collagen-Based Biomaterials for Tissue Engineering. *ACS Biomaterials Science & Engineering* **2023**, *9* (3), 1132-1150. DOI: 10.1021/acsbiomaterials.2c00730.

(59) Cao, H.; Xiang, D.; Zhou, X.; Yue, P.; Zou, Y.; Zhong, Z.; Ma, Y.; Wang, L.; Wu, S.; Ye, Q. High-Strength, Antibacterial, Antioxidant, Hemostatic, and Biocompatible Chitin/Pegde-Tannic Acid Hydrogels for Wound Healing. *Carbohydrate Polymers* **2023**, *307*, 120609. DOI: https://doi.org/10.1016/j.carbpol.2023.120609.

(60) Yu, R.; Yang, Y.; He, J.; Li, M.; Guo, B. Novel Supramolecular Self-Healing Silk Fibroin-Based Hydrogel via Host–Guest Interaction as Wound Dressing to Enhance Wound Healing. *Chemical Engineering Journal* **2021**, *417*, 128278. DOI: https://doi.org/10.1016/j.cej.2020.128278.

(61) Han, X.; Chen, S.; Cai, Z.; Zhu, Y.; Yi, W.; Guan, M.; Liao, B.; Zhang, Y.; Shen, J.; Cui, W.; et al. A Diagnostic and Therapeutic Hydrogel to Promote Vascularization via Blood Sugar Reduction for Wound Healing. *Advanced Functional Materials* **2023**, *33* (14), 2213008. DOI: https://doi.org/10.1002/adfm.202213008.

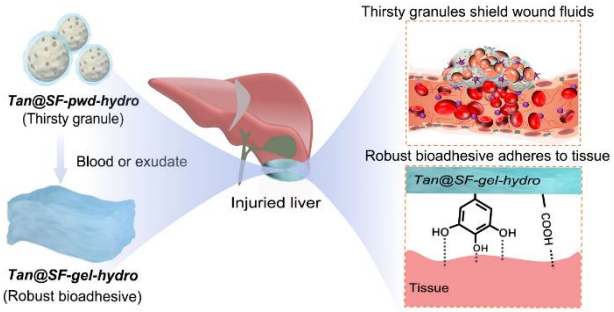

Turn adversity (over wetness) into opportunity (wet adhesion)

For Table of Contents Only